



1 **Aerosol pH Indicator and Organosulfate Detectability from Aerosol Mass Spectrometry**

2 **Measurements**

3 Melinda K. Schueneman¹, Benjamin A. Nault¹, Pedro Campuzano-Jost¹, Duseong S. Jo^{1,2},
4 Douglas A. Day¹, Jason C. Schroder^{1,*}, Brett B. Palm¹, Alma Hodzic², Jack E. Dibb³, and Jose L.
5 Jimenez¹

6

7 [1] Department of Chemistry, and Cooperative Institute for Research in Environmental Sciences
8 (CIRES), University of Colorado, Boulder, CO, USA

9 [2] Atmospheric Chemistry Observations and Modeling, National Center for Atmospheric
10 Research, Boulder, CO 80301, USA

11 [3] Earth Systems Research Center, Institute for the Study of Earth, Oceans, and Space,
12 University of New Hampshire, USA

13

14 * Now at: Air Pollution Control Division, Colorado Department of Public Health and the
15 Environment, Denver, CO, USA

16

17 Correspondence: jose.jimenez@colorado.edu

18

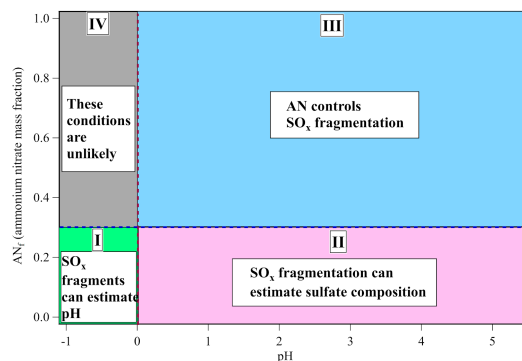


19 Abstract

20

21 Aerosol sulfate is a major component of submicron particulate matter (PM_{10}). Sulfate can be
22 present as inorganic (mainly ammonium sulfate, AS) or organic sulfate (OS). Although OS are
23 thought to be a smaller fraction of total sulfate in most cases, recent literature argues that this
24 may not be the case in more polluted environments. Aerodyne Aerosol Mass Spectrometers
25 (AMS) measure total submicron sulfate, but it has been difficult to apportion AS vs. OS as the
26 detected ion fragments are similar. Recently, two new methods have been proposed to quantify
27 OS separately from AS with AMS data. We use observations collected during several airborne
28 field campaigns covering a wide range of sources and air mass ages (spanning the continental US,

29 marine remote troposphere, and Korea) and
30 targeted laboratory experiments to investigate
31 the performance and validity of the proposed
32 OS methods. Four chemical regimes are
33 defined to categorize the factors impacting
34 sulfate fragmentation (Fig. shown in abstract).
35 In polluted areas with high ammonium nitrate
36 concentrations and in remote areas with high
37 aerosol acidity, the decomposition and
38 fragmentation of sulfate in the AMS is
39 influenced by multiple complex effects, and
40 estimation of OS does not seem possible with



41 current methods. In regions with lower acidity ($pH > 0$) and ammonium nitrate (fraction < 0.3), the
42 proposed OS methods might be more reliable, although application of these methods often
43 produced nonsensical results. However, the fragmentation of ambient neutralized sulfate varies
44 somewhat within studies, adding uncertainty, possibly due to variations in the effect of organics.
45 Under highly acidic conditions, sulfate fragment ratios show a clear relationship with acidity (pH
46 and ammonium balance). The measured ammonium balance (and to a lesser extent, the
47 $H_ySO_x^+ / SO_x^+$ AMS ratio) is a promising indicator for rapid estimation of aerosol $pH < 0$,
48 including when gas-phase NH_3 and HNO_3 are not available. These results allow an improved
49 understanding of important intensive properties of ambient aerosols.

50



51 **Introduction**

52 PM_{10} , or submicron aerosols, have important impacts on visibility, climate, and
53 environmental and human health (Dockery et al., 1996; Lighty et al., 2000; Lohmann et al.,
54 2004; IPCC, 2013). In order to quantify the impacts of PM_{10} , and their evolution with changes in
55 emissions, chemistry, and climate, PM_{10} sources, chemistry, and composition must be understood.
56 Field measurements are critical to that goal, and one tool used extensively in field studies since
57 the early 2000s is the Aerodyne Aerosol Mass Spectrometer (AMS) and more recently its
58 simplified version, the Aerosol Chemical Speciation Monitor (ACSM) (Jayne et al., 2000;
59 DeCarlo et al., 2006; Canagaratna et al., 2007; Ng et al., 2011a)). The AMS typically quantifies
60 the chemical composition and size distribution of sulfate, nitrate, organic aerosol (OA),
61 ammonium, and chloride (Jayne et al., 2000; DeCarlo et al., 2006; Canagaratna et al., 2007;
62 Jimenez et al., 2009)

63 Within the AMS, particles are vaporized, leading to some thermal decomposition (e.g.,
64 (Docherty et al., 2015) and then ionized via 70 eV electron ionization, which leads to substantial
65 fragmentation of the molecular ions. Despite or perhaps because of the substantial (and
66 reproducible) decomposition and fragmentation, the relative signals of different AMS fragments
67 have been found to be indicative of different chemical species in the aerosol. These include the
68 presence of inorganic vs. organic nitrates (Farmer et al., 2010; Fry et al., 2013), and of several
69 source and composition characteristics of organic aerosols (Alfarra et al., 2004; Zhang et al.,
70 2004a; Cubison et al., 2011; Ng et al., 2011b; Hu et al., 2015). In contrast to nitrates,
71 deconvolving inorganic vs. organic sulfates is thought to be more difficult, as the fragmentation
72 pattern for one atmospherically relevant organosulfate (OS) was similar to those of inorganic



73 sulfates (mainly ammonium-sulfate salts, AS) in an early study, with minimal C-S-containing
74 fragments (Farmer et al., 2010). Until recently, most studies have shown that the OS molar
75 fraction ($OS_f = OS / (AS + OS)$, calculated using only the sulfate moiety of the molecules)
76 typically makes a small (~1-10%) contribution to total sulfate in PM_{10} (e.g. (Tolocka and Turpin,
77 2012; Hu et al., 2015; Liao et al., 2015; Riva et al., 2016, 2019a)). However, for biogenic areas
78 OS_f is predicted to increase substantially in the future (Riva et al., 2019b). Another important
79 recent subject of debate is the missing sulfate production in haze events in China (Wang et al.,
80 2014; Zheng et al., 2014; Li et al., 2017), which some studies have attributed to a major
81 contribution of OS (e.g., (Song et al., 2019)). It is also important to quantify OS in order to
82 understand the chemistry of aerosol formation and aging (Surratt et al., 2007, 2008; Song et al.,
83 2019), which impacts the ability to understand how sulfate may influence various PM_{10} properties
84 and processes (e.g., gas uptake, aqueous reactions). Finally, accurate AS concentrations are
85 needed to quantify the inorganic:organic ratio (to predict the hygroscopicity of PM_{10} , which
86 impacts satellite and model interpretation) and to estimate aerosol pH and liquid water content
87 from thermodynamic models, as it is currently still not possible to measure the aerosol pH in the
88 field in-situ (Hennigan et al., 2015; Guo et al., 2016; Craig et al., 2018; Pye et al., 2019).

89 Recent AMS work has attempted to quantify OS_f from the measured individual sulfate
90 ion signals. The vaporization and ionization of AS and OS in the AMS produces almost
91 exclusively “inorganic” ion fragments, the major ones quantified being SO^+ , SO_2^+ , SO_3^+ , HSO_3^+ ,
92 and $H_2SO_4^+$ (Farmer et al., 2010). Note that these are the ions detected in the AMS (following
93 ionization/decomposition), and not the ions present in the aerosols (discussed in Sect. 3.2 and
94 shown in Fig. 2C). However, recent laboratory studies with many OS standards have found



95 reproducible differences in the fragmentation of AS vs OS (Chen et al., 2019). That study
96 proposed a method using the unique AS ion fragments (H_2SO_4^+ and HSO_3^+) divided by the total
97 sulfate signal ($\text{H}_2\text{SO}_4^+ + \text{HSO}_3^+ + \text{SO}_3^+ + \text{SO}_2^+ + \text{SO}^+$) to apportion OS, AS, and methylsulfonic acid
98 (MSA, an organosulfur compound, but not an organosulfate) in field datasets. It is important to
99 note that MSA can be directly measured with the (HR-)AMS (Phinney et al., 2006; Zorn et al.,
100 2008; Huang et al., 2017; Hodshire et al., 2019), so quantification of MSA with the method in
101 Chen et al. is not necessary. From this method, an average OS mass concentration (C_{OS}) of 0.12
102 $\mu\text{g m}^{-3}$ was estimated for the SOAS ground campaign in rural Alabama (Carlton et al., 2018),
103 with $\text{OS}_f \sim 4\%$ (Chen et al., 2019). That estimate is consistent with others for that site and region
104 (Hu et al., 2015; Liao et al., 2015). An alternative method to estimate OS_f based on the same
105 principle was proposed by Song et al. (2019) using the observed AMS $\text{SO}^+/\text{H}_y\text{SO}_x^+$ and
106 $\text{SO}_2^+/\text{H}_y\text{SO}_x^+$. These authors reported $\text{OS}_f \sim 17\% \pm 7\%$ (which corresponds to $[\text{OS}] \sim 5\text{-}10 \mu\text{g m}^{-3}$)
107 during winter haze episodes in China, based on their method. A recent study (Dovrou et al.,
108 2019) investigated mixtures of sodium sulfate and sodium hydroxymethanesulfonate (HMS);
109 however, they found that HMS cannot be distinguished from AMS ions alone, due to the
110 complex ambient aerosol mixture containing organic sulfates, and inorganic sulfates, which all,
111 in part, produce the same sulfate fragments as HMS.

112 Another important and related analytical challenge is online quantification or estimation
113 of ambient aerosol acidity from real-time measurements, e.g. during field campaigns. So far,
114 online aerosol pH measurements have only been performed in the laboratory (Rindelaub et al.,
115 2016; Craig et al., 2018). Aerosol acidity is important because it impacts human health by
116 decreasing lung function (Raizenne et al., 1996), and strongly impacts the equilibria and kinetics



117 of a very large number of atmospheric physical and chemical processes (Jang et al., 2002;
118 Meskhidze et al., 2003; Anon, 2007; Thornton et al., 2008; Bertram and Thornton, 2009; Gaston
119 et al., 2014; Ackendorf et al., 2017; Guo et al., 2017; Losey et al., 2018). In addition, the
120 deposition of acidic particles leads to damage to terrestrial and freshwater ecosystems, i.e. “acid
121 rain” or more properly acid deposition (Schindler, 1988; Johnson et al., 2008). Currently, the
122 state-of-the art technique to quantify aerosol acidity for field data is to run an inorganic aerosol
123 thermodynamic model that includes the measured particle and gas inorganic concentrations, as
124 well as temperature and humidity. The Extended Aerosol Inorganics Model (E-AIM) (Clegg et
125 al., 1998a, 2003; Wexler and Clegg, 2002) is generally considered as the reference model (Pye et
126 al., 2019). ISORROPIA-II (Nenes et al., 1999; Fountoukis and Nenes, 2007) is a faster model
127 utilizing look-up tables to calculate aerosol liquid water content (and thus is frequently used as
128 part of chemical transport models) at the expense of some accuracy at different RH levels (Pye et
129 al., 2019). In general, these thermodynamic models are thought to perform best for pH
130 estimation when gas-phase measurements of NH_3 and/or HNO_3 are used in the calculations, and
131 to perform less well when run only with aerosol measurements (Guo et al., 2015; Hennigan et
132 al., 2015; Song et al., 2018).

133 There has been an ongoing debate about the potential relationship between the inorganic
134 cation/anion charge ratio (commonly referred to as “ammonium balance”, see Eq. (4)) and
135 aerosol acidity. Ammonia gas and its particle phase equivalent (ammonium) are the dominant
136 bases in the atmosphere (Dentener and Crutzen, 1994). As the most important base in PM_{10} , a
137 deficit of NH_4^+ vs. dominant PM_{10} anions, SO_4^{2-} and NO_3^- (Jimenez et al., 2009), is indicative of
138 the concentration of H^+ , since the particles are (nearly) electrically neutral. Thus, in the absence



139 of substantial non-volatile cations (e.g. Na^+ , K^+) ammonium balance is an indicator of aerosol
140 acidity. Ammonium balance has been shown to correlate well with pH under certain conditions,
141 specifically, when using daily averaged temperature and relative humidity (Zhang et al., 2007a),
142 but has been criticized as being a poor surrogate of pH under other conditions (Hennigan et al.,
143 2015). In particular, ammonium balance can be a poor surrogate of pH because changes in T and
144 RH impact the aerosol liquid water in the diurnal cycle (Zhang et al., 2007a). This is especially
145 important in the boundary layer where almost all past pH quantification has been carried out
146 (Pye et al., 2019), compared to the lower diurnal variance of T and RH in the free and upper
147 troposphere. Many field studies do not include measurements of NH_3 or HNO_3 , sticky species
148 present at low concentrations and thus not routinely measured, limiting the ability to calculate
149 aerosol pH (Hennigan et al., 2015). A more direct estimate of aerosol acidity using only ambient
150 particle data is highly desirable.

151 Here, we analyze sulfate ion fragment data from laboratory and ambient AMS
152 observations, spanning multiple aircraft campaigns with a routinely calibrated AMS response to
153 AS, and across a wide range of chemical and meteorological environments. We use this large
154 dataset to test the applicability of recently published methods to partition AS and OS. We
155 investigate the feasibility of estimating pH based on AMS data; as well as the regions of
156 chemical space where the different estimation methods may work. Finally, we provide a physical
157 interpretation for sulfate fragmentation in the AMS.

158

159 **2 Methods**

160 **2.1 Airborne Campaigns**



161 Sulfate fragmentation data was obtained using an Aerodyne High-Resolution
162 Time-of-Flight Aerosol Mass Spectrometer (AMS) (Aerodyne Research Inc., Billerica, MA,
163 USA; (DeCarlo et al., 2006)). The ambient data used here are from aircraft observations from the
164 following campaigns (Table 1): DC3 (Barth et al., 2015), SEAC⁴RS (Toon et al., 2016),
165 WINTER (Schroder et al., 2018), KORUS-AQ (Nault et al., 2018), and ATom-1 and ATom-2
166 (Guo et al., 2020; Hodzic et al., 2020)). Flight paths for all six campaigns are shown in Fig. S1.
167 These campaigns span polluted urban, partially polluted biogenic, biomass burning smoke, rural,
168 and remote regions of the atmosphere. DC3 sampled continental / rural conditions with diffuse
169 pollution and some biomass burning events. WINTER and KORUS-AQ were airborne
170 campaigns that focused on urbanized regions (although from different regions and times of year
171 (Table 1)); therefore, the campaigns had appreciable mass concentrations of ammonium nitrate
172 due to anthropogenic emissions of NO_x and the subsequent production of HNO₃ that partitions
173 into the aerosol with ammonia (Seinfeld and Pandis, 2006). SEAC⁴RS focused on regional
174 background chemistry of the continental United States, which included impacts from biomass
175 burning, biogenic, and pollution emissions, and upper tropospheric chemistry impacted by
176 convection. Finally, ATom-1 and ATom-2 sampled the remote Pacific and Atlantic basins with
177 continuous full vertical profiling, in order to study the composition of the remote marine
178 atmosphere, impacted by long range transported chemical species and marine emissions, and far
179 from anthropogenic sources. Not all campaigns are usable for all the analyses in this paper,
180 depending on the quality and completeness of the data. Table 1 indicates which campaigns were
181 usable for each analysis.

182



183 **2.2 High-Resolution Time-of-Flight Aerosol Mass Spectrometer**

184 The highly customized University of Colorado-Boulder aircraft AMS was used in all
185 campaigns and has been described elsewhere (DeCarlo et al., 2008; Dunlea et al., 2009; Nault et
186 al., 2018; Schroder et al., 2018; Guo et al., 2020), so only details relevant to this study are
187 summarized here. Ambient air is drawn through a National Center for Atmospheric Research
188 (NCAR) High-Performance Instrumented Airborne Platform for Environmental Research
189 Modular Inlet (HIMIL: (Stith et al., 2009)) with a constant standard flow rate of 9 L min⁻¹, and
190 all data is reported at a constant standard temperature ($T = 273$ K) and pressure ($P = 1013$ hPa).
191 The sampled air enters a pressure controlled inlet (Bahreini et al., 2008) and is then introduced
192 into an aerodynamic focusing lens (Liu et al., 1995; Zhang et al., 2004b). Particles then impact
193 onto an inverted cone porous tungsten “standard” vaporizer, operated at ~ 600 °C under high
194 vacuum. The standard vaporizer is used in this study. A “capture vaporizer” has been recently
195 demonstrated, it leads to more thermal decomposition while still retaining similar (although
196 noisier) fragment information (Hu et al., 2017a; Zheng et al., 2020), but it is not used here.
197 Non-refractory species, those that evaporate in less than a few seconds (such as sulfate, nitrate,
198 ammonium, and organic material), are subsequently ionized by 70 eV electrons. Some refractory
199 and semi-refractory species such as sea-salt, lead and potassium can be detected by the AMS in
200 some cases (Lee et al., 2010; Salcedo et al., 2010; Ovadnevaite et al., 2012; Hodzic et al., 2020)).
201 A cryopump reduces background in the ionizer by orders of magnitude during the flights, leading
202 to low detection limits, in particular for NH₄, which is critical for acidity quantification in the
203 remote troposphere. Data was taken at 1 Hz, but was processed at both 1 Hz and 1 minute
204 resolution, and the latter product is primarily used here due to higher signal-to-noise ratios. The



205 one minute datasets were further filtered by removing points where the sulfate signal was below
206 three times its detection limit. Detection limits were estimated continuously via the methods of
207 Drewnick et al. (2009), and confirmed with frequent in-flight filter blanks. For the laboratory
208 studies, everything was kept the same as on the aircraft other than no use of the HIMIL aircraft
209 inlet. Data was processed and analyzed with the standard Squirrel and PIKA ToF-AMS data
210 analysis software packages within Igor Pro 7 (Wavemetrics) (DeCarlo et al., 2006; Sueper,
211 2018).

212 One important parameter for AMS quantification is collection efficiency (CE). CE is the
213 probability that a particle entering the AMS is detected. It is affected by several particle
214 properties (Huffman et al., 2005), the most important being particle bounce off the vaporizer
215 without detection (Middlebrook et al., 2012). Bounce is controlled by particle phase (Quinn et
216 al., 2006; Matthew et al., 2008), and is estimated for ambient particles based on their ammonium
217 balance (acidity) and ammonium nitrate content (Middlebrook et al., 2012). This
218 parameterization performs well for ambient particles (Middlebrook et al., 2012; Hu et al., 2017a,
219 2020; Guo et al., 2020). Still, potential variability in CE that is not perfectly captured by the
220 parameterization contributes a major fraction of the AMS uncertainty for ambient particle
221 analysis (Bahreini et al., 2009). Alternative methods to estimate ambient CE for ambient
222 particles are of interest.

223

224 **2.3 Quantification of OS/AS using Literature Methods**

225 Two methods have been proposed to quantify OS contribution to total sulfate using AMS
226 sulfate ion fragment fractions. The first method uses different sulfate ions to attribute measured



227 total sulfate to either OS, AS, or methanesulfonic acid (MSA). Due to the structure of OS, only
228 non-hydrogenated sulfate ions, i.e., SO^+ , SO_2^+ and SO_3^+ , are produced in the AMS for OS. AS
229 does produce hydrogenated sulfate ions, i.e., H_2SO_4^+ and HSO_3^+ , as well as the same
230 non-hydrogenated sulfate ions produced by OS. Chen et al. (2019) proposed a “triangle method”
231 to estimate these two species and MSA, based on the observed fragments. Note that mineral
232 sulfates such as sodium sulfate fragment similarly to OS, and thus these methods need to be
233 interpreted differently in regions with significant submicron mineral sulfates. MSA calibrations
234 show variability for the fragments (Chen et al., 2019), and were not performed for all the studies
235 in this work. Since MSA can be quantified without using the sulfate fragments, here we apply
236 this method to estimate the fractions of OS and AS by using a one dimensional version of the
237 triangle (i.e. just the hypotenuse connecting pure OS to pure AS). An alternative method is
238 based on the same assumptions, but uses different equations to quantify the relative
239 concentration of OS (Song et al., 2019).

240 Both literature methods for deconvolving sulfate as OS and AS assume that the main
241 factor impacting sulfate fragmentation in the AMS is sulfate structure (OS, AS, or MSA). Chen
242 et al. (2019) briefly mention that acidity can impact sulfate fragmentation, but this effect has not
243 been studied and quantified. In addition, Chen et al. (2019) used pure standards to quantify the
244 AMS fragmentation of different species, but did not explore potential matrix effects in AMS
245 fragments which could impact internally mixed ambient particles.

246

247 **2.4 Quantification of the AMS Sulfate Fragment Ratios**



248 To compare our field data to that analyzed in Chen et al. (2019) we use the variables
249 defined in that study, $fH_2SO_4^+$ and $fHSO_3^+$ and define the normalized $nfH_2SO_4^+$ and $nfHSO_3^+$
250 (normalized to the values of $fH_2SO_4^+$ and $fHSO_3^+$ for pure AS) :

251

$$fH_2SO_4^+ = \frac{[H_2SO_4^+]}{[H_2SO_4^+] + [HSO_3^+] + [SO_3^+] + [SO_2^+] + [SO^-]} \quad \text{Eq. 1}$$

252

$$nfH_2SO_4^+ = \frac{fH_2SO_4^+}{fH_2SO_4^+ (\text{pure AS})} \quad \text{Eq. 2}$$

253

$$fHSO_3^+ = \frac{[HSO_3^+]}{[H_2SO_4^+] + [HSO_3^+] + [SO_3^+] + [SO_2^+] + [SO^-]} \quad \text{Eq. 3}$$

254

$$nfHSO_3^+ = \frac{fHSO_3^+}{fHSO_3^+ (\text{pure AS})} \quad \text{Eq. 4}$$

255

256 It should be noted that while that study includes methanesulfonic acid (MSA) data, the impact of
257 MSA on $fH_2SO_4^+$ and $fHSO_3^+$ is minimal for the ATom campaigns (see Fig. S2). Additionally,
258 one study over the Western United States (representing a rural, continental region) observed
259 MSA concentrations of $\sim 50 \text{ ng m}^{-3}$ (Sorooshian et al., 2015), which results in a very small
260 deviation in the Chen triangle and can hence be neglected for the purposes of this work. All



261 variables were normalized to the values of the same variables for pure AS calibrations
262 (conducted during each field experiment) in order to eliminate some of the spread in the sulfate
263 ions that is likely due to instrument-to-instrument or instrument-in-time variability (Fry et al.,
264 2013; Chen et al., 2019) (Fig. S3) . We also define a new AMS sulfate ion ratio, $H_ySO_x^+/SO_x^+$, as
265 and create the normalized $nH_ySO_x^+/SO_x^+$ to reduce the influence of instrument-instrument
266 variability:

$$H_ySO_x^+/SO_x^+ = \frac{[H_ySO_x^+]}{[SO_x^+]} = \frac{[H_2SO_4^+]+[HSO_3^+]}{[SO_3^+]+[SO_2^+]+[SO^+]} \quad \text{Eq. 5}$$

267

$$nH_ySO_x^+/SO_x^+ = \frac{H_ySO_x^+/SO_x^+}{H_ySO_x^+/SO_x^+ (\text{pure AS})} \quad \text{Eq. 6}$$

268

269 The submicron aerosol molar Ammonium Balance (NH_{4_bal}) is calculated as:

270

$$NH_{4_bal} = \frac{[NH_4]/18}{([SO_4]/48)+([NO_3]/62)+([Chl]/35)} \quad \text{Eq. 7}$$

271

272 The concentration of non-refractory chloride is only included for non-remote campaigns
273 (KORUS-AQ, WINTER, and SEAC⁴RS), since it was negligible for others and strongly
274 impacted by seasalt in the marine boundary layer. The fraction of ammonium nitrate in the
275 particle phase (ammonium nitrate mass fraction, AN_f) (by mass):

$$AN_f = \frac{(80 \div 62) \times [Inorganic NO_3]}{[NO_3]+[SO_4]+[NH_4]+[Chl]+[Org]} \quad \text{Eq. 8}$$



276

277 The fraction of total AMS aerosol mass comprised of OA (OA_f) is:

$$OA_f = \frac{[Org]}{[NO_3] + [SO_4] + [NH_4] + [Chl] + [Org]} \quad \text{Eq. 9}$$

278

279 The sulfate equivalent concentration of OS in the Song et al. (2019) paper is calculated as:

$$C_{OS} = M_{SO_4} \left[\frac{SO_{cd, SO^+ / H_y SO_x^+}^{obs-R} \cdot H_y SO_{x, obs}^+}{M_{SO^+}} + \frac{SO_{cd, SO_2^+ / H_y SO_x^+}^{obs-R} \cdot H_y SO_{x, obs}^+}{M_{SO_2^+}} \right] \quad \text{Eq. 10}$$

280

281 where “cd” stands for “clean and dry”. Clean and dry conditions are defined in Song et al. (2019)

282 as ambient data points where $PM_{10} = 10 \mu\text{g m}^{-3}$ and $RH = 30\%$. Clean and dry conditions are

283 assumed to represent nearly pure AS. M is for the molar mass of the different sulfate ions, and

284 “obs” represents the ambient data for specific sulfate fragments. $H_y SO_x^+$ is defined in Song et al.

285 (2019) as $(SO_3^+ + HSO_3^+ + H_2SO_4^+)$. For the Chen method, the C_{OS} is defined based on the AS

286 normalized $nfH_2SO_4^+$ values:

287

$$C_{OS} = [SO_4] - nfH_2SO_4^+ * [SO_4] \quad \text{Eq. 11}$$

288

289 OS_f , the fraction of OS:total sulfate is defined as:

290

$$OS_f = \frac{C_{OS}}{[SO_4]} \quad \text{Eq. 12}$$



291 Where C_{OS} is calculated from Eq. (10) or Eq. (11).

292

293 **2.5 Laboratory Experiments**

294 As ambient aerosols contain mixtures of chemical species, we investigated if matrix
295 effects may impact the fragmentation of sulfate species. Different solution mixtures, composed
296 of various amounts of AS (Certified ACS, 99.7% purity) and ammonium nitrate (AN) (Certified
297 ACS, 99.9% purity) in water (Milli-Q grade ($R > 19$ MOhms)) were atomized to generate
298 particles and size selected using a Differential Mobility Analyzer (DMA) (TSI Model 3081),
299 analyzed with a Condensation Particle Counter (CPC) (Model 3775), and electrostatic classifier
300 (Model 3080), for mobility diameters between 350-400 nm. We investigated AS/AN mixtures,
301 ranging from $AN_f = 0\%$ to 95%.

302 In order to assess effects on the sulfate fragmentation from mixing with OA, chamber
303 experiments, where different types of SOA were formed by gas-phase reactions and
304 condensation onto AS seeds, were investigated. SOA was formed from alkanol and toluene
305 photooxidation under high- NO_x conditions (Liu et al., 2019), as well as Δ -3-carene and α -pinene
306 reactions with nitrate radicals (Kang et al., 2016) Experiments were initiated with 100% AS in a
307 dry chamber ($RH < 5\%$; ~ 298 K) followed by either rapid, gradual, or stepwise increases of
308 SOA until a maximum OA/(OA+AS) ratio of $\sim 70\%$ was reached. Aerosol composition was
309 monitored by AMS and size distributions were monitored with a scanning mobility particle sizer
310 (SMPS, TSI). RIE of sulfate was directly calibrated with pure ammonium sulfate, while RIE *
311 CE of the SOA produced was estimated by comparison to the SMPS integrated volume, together
312 with OA density estimated from the AMS-derived elemental ratios per Kuwata et al. (2012)), in



313 order to accurately quantify OA/(OA+AS). Humid experiments were not considered here due to
314 the potential of forming organosulfates.

315

316 ***2.6 E-AIM Thermodynamic Model for pH Estimation***

317 Aerosol pH was estimated using the Extended Aerosol Inorganic Model (E-AIM) Model
318 IV (Clegg et al., 1998b; Massucci et al., 1999; Wexler and Clegg, 2002). We input into the model
319 the total nitrate (gas and particle phase), particle phase ammonium and sulfate, and ambient T
320 and RH to calculate aerosol liquid water and aerosol pH. Model IV is not run with chloride ions,
321 as their concentrations were very low, and including chloride limits the model to temperatures \geq
322 263 K (Friese and Ebel, 2010), which would greatly limit the analysis of pH for WINTER,
323 ATom-1, and ATom-2. Also, including chloride precludes running the model under
324 supersaturated solution conditions, which is a closer approximation of ambient aerosol (Pye et
325 al., 2019). The model was run in the “forward mode,” meaning that total nitrate (gas-phase
326 HNO_3 plus particle-phase total NO_3^-), sulfate, ammonium, relative humidity (calculated
327 according to the parameterization of Murphy and Koop (2005) which is critical for upper
328 tropospheric conditions), and temperature were input into the model. All aerosol mass
329 concentrations were from the CU AMS. $\text{HNO}_3(\text{g})$ was measured by the California Institute of
330 Technology chemical ionization mass spectrometer (CIT-CIMS) (Crouse et al., 2006), which
331 was flown in all of these missions (excluding WINTER, where the UW-CIMS was used for the
332 HNO_3 measurements) (Lee et al., 2014, 2018). Results are generally similar when using the
333 SAGA mist chamber measurement for total nitrate (Nault et al., 2020). The forward mode is less
334 sensitive to uncertainties in measurements than the “reverse mode,” which only uses particle



335 composition and T/RH as inputs (Hennigan et al., 2015). Also, due to lack of $\text{NH}_3(\text{g})$
336 measurements, the model was run iteratively until convergence in modeled NH_3 occurred,
337 similar to Guo et al. (2016). Performance for modeled pH was investigated by comparing
338 model-calculated HNO_3 and NO_3^- to measurements, as the partitioning of nitrate between gas-
339 and particle-phase is sensitive to pH under acidic conditions (Guo et al., 2016). For all
340 campaigns included herein (DC3, WINTER, SEAC⁴RS, KORUS-AQ, ATom-1, and ATom-2),
341 the slopes of HNO_3 (measured vs. predicted) are within the uncertainty of the measurements;
342 with good correlations (SI Fig. S4). For NO_3^- , the slopes are within the measurement uncertainty
343 for five of the six campaigns. For ATom-2, the NO_3^- slopes were low; however, for this
344 campaign, the measured NO_3^- mass concentrations were extremely low (mean = $0.02 \mu\text{g sm}^{-3}$),
345 and the pH was also very low (mean = -0.5), leading to very little NO_3^- in the aerosol phase (see
346 SI Fig. S4).

347 In addition, other bases present in the atmosphere (such as amines) were examined. Prior
348 studies have shown that amines were less than a maximum concentration of 30 ng m^{-3} at the
349 ocean surface (Gibb et al., 1999; Facchini et al., 2008; Müller et al., 2009; Frossard et al., 2014;
350 van Pinxteren et al., 2015; Youn et al., 2015). Another study found that amine mass
351 concentration dropped off quickly with altitude to concentrations less than 10 ng m^{-3} at the
352 altitude that the DC-8 flew over marine surfaces (Sorooshian et al., 2009). As the one minute
353 detection limit for the AMS data for amines is typically 10 ng m^{-3} , we expect the amine signal to
354 generally be below the limit of detection, and thus outside of our quantification capabilities. This
355 was observed for AMS data from the ATom campaigns, using characteristic ions identified in
356 past studies (Murphy et al., 2007; Ge et al., 2014). It was found that amine ions cannot be



357 distinguished from background for many ATom flights. Only during one flight in ATom-1, we
358 observed an amine signal ($C_2H_6N^+$ $m/z = 44$) above the background (see SI Fig. S5). During this
359 flight, amines (from the contribution of CH_4N , C_2H_6N , and C_3H_8N) only accounted for 0.7 ng
360 m^{-3} of aerosol, whereas ammonium accounted for 19 ng m^{-3} . Amines can produce the same
361 fragments as ammonium, but this is only the case for a few percent of the amine fragments (Ge
362 et al., 2014). In this case, the ammonium concentration is 25 times that of the amines. Since
363 amines were even lower during other flights, we assume the effect of amines to the pH
364 calculation is very small and can be ignored for E-AIM calculations.

365

366 2.7 GEOS-Chem Model

367 We used a global chemical transport model (GEOS-Chem 12.6.1,
368 doi:10.5281/zenodo.3520966; (Bey et al., 2001)) to investigate modeled global distributions of
369 ammonium nitrate mass fraction (AN_p) and aerosol pH across different regions. GEOS-Chem
370 was driven by assimilated meteorological fields from the Modern-Era Retrospective analysis for
371 Research and Applications version 2 (MERRA2) (Gelaro et al., 2017) for the year of 2010. The
372 simulation was conducted at 2° (latitude) \times 2.5 (longitude) with 47 vertical layers up to 0.01 hPa
373 and \sim 30 layers under 200 hPa. We used the Community Emissions Data System (CEDS)
374 inventory for global anthropogenic emissions (Hoesly et al., 2018) and the global fire emissions
375 database version 4 (GFED4) for biomass burning emissions (Giglio et al., 2013). Aerosol pH and
376 gas-particle partitioning of inorganic aerosols were calculated online using the ISORROPIA-II
377 model within GEOS-Chem (Fountoukis and Nenes, 2007; Pye et al., 2009). Similar to Jo et al.,
378 (2019) sea salt aerosol was excluded from pH calculations based on a better agreement with the



379 observationally-constrained pH values as suggested by Nault et al. (2020). GEOS-Chem includes
380 sea salt aerosol in ISORROPIA calculation but we excluded sea salt aerosol based on Nault et al.
381 (2020). Oceanic NH_x emissions were also included in this model based on recent work (Paulot et
382 al., 2015; Nault et al., 2020).

383

384 **3 Results and Discussion**

385 **3.1 Lab quantification of AMS data**

386 Application of the one dimensional Chen method to laboratory data is shown in Fig. 1.
387 Data are expected to lie inside the triangular region, and be apportioned depending on the
388 relative distance to the three vertices. For example, data lying at [0.5,0.5] on the line between the
389 OS and AS points would represent a sample with ~50% OS and ~50% AS. If data clusters
390 around the [1,1] point where pure AS resides, all of the sulfate is attributed to AS.

391 The effect of internally mixed ammonium nitrate (AN) is shown in Fig. 1A. For mixtures
392 containing $\text{AN}_f < 50\%$, data centers around the pure AS point in the Chen triangle. When AN_f is
393 increased past 0.50, there is an increase in both $\text{NH}_4^+\text{SO}_4^-$ ions. For example, an aerosol with AN_f
394 = 0.75 results in $\text{OS}_f = -11\%$ with the Chen method, which is nonsensical. When $\text{AN}_f = 0.90$, OS_f
395 = -33%, and when $\text{AN}_f = 0.95$, $\text{OS}_f = -50\%$. This indicates that in a sample containing some
396 mixture of OS, AS, and AN, the total sulfate would need to be 50% OS and 50% AS (at $\text{AN}_f =$
397 0.95) to give a non-negative OS_f . Thus for laboratory data, the Chen method should not be used
398 on mixtures containing $\text{AN}_f > 0.50$.

399 The effect of OA internally mixed with AS on the sulfate fragmentation pattern was also
400 explored with toluene, alkanol, and monoterpene SOA. For the alkanol SOA experiments we



401 found that the presence of even a small coating of alkanol SOA (which is thought to be liquid
402 (Liu et al., 2019)) shifts the normalized AS [1,1] point to $\sim[1.08,1.08]$, but increases in the
403 fraction of OA (OA_f) from 0.1 to 0.3 lead to no further changes in $nfH_ySO_x^+$ (Fig. 1B). This
404 means that for a sample containing a mixture of AS and alkanol SOA, the calculated OS_f would
405 be -15% (Chen). In contrast, toluene SOA, which spans $0 < OA_f < 0.5$, shows no clear change in
406 the $nfH_ySO_x^+$ ions, indicating that OA_f would not bias the Chen method for this example. The
407 monoterpene SOA, from two different experimental datasets using different AMSs, show more
408 varied results than the previous two studies. Overall, in the OA_f range 0-0.50, the 2015
409 monoterpene data shows a consistent and constant 10-20% increase in $nfH_ySO_x^+$ compared to the
410 pure AS calibration point (similarly to the alkanol SOA). However, when OA_f is in the range of
411 $0.50 < OA_f < 0.70$, 30-40% increases are observed. This result is only applicable to a few of the
412 experiments (see Fig. S6), potentially due to very high SOA loadings (up to $300 \mu\text{g m}^{-3}$). These
413 high OA concentrations could potentially lead to a change of the particle phase due to
414 condensation of more volatile and liquid species, potentially altering the interactions of the
415 particles and the vaporizer surfaces.

416 These experiments collectively suggest that a “pure” AS calibration point of [1.15,1.15]
417 may be more appropriate when applying the Chen et al. method to some mixed aerosol at typical
418 OA concentrations observed in the atmosphere.

419 Chen et al. briefly discussed the potential impact of acidity on their OS quantification
420 method. This is explored here with pure sulfuric acid lab calibrations (Fig. 1C). Pure sulfuric
421 acid shows a large deviation from the pure AS triangle point (similar to increasing AN_f), nearly



422 doubling the values for the $\eta H_y SO_x^+$ ions. This implies that a particle containing sulfuric acid
423 would produce a strong negative bias on the estimate of OS by the Chen method.

424

425 **3.2 Physical Interpretation of the Sulfate Fragmentation Trends**

426 It is useful to provide a physical interpretation of the trends that are likely driving the
427 observed sulfate fragmentation changes, based on the physicochemical details of the AMS
428 detection and those of the particles being sampled. In Fig. 2A, a simplified diagram of the AMS
429 detection process is shown, highlighting important details that are thought to give rise to the
430 observed trends.

431 Ambient particles containing AS, OS, and other species are sampled into the AMS
432 through a focusing lens. Following a series of differential pumping steps through the instrument,
433 the particles impact on a porous tungsten standard vaporizer. The time spent under vacuum from
434 sampling to detection is of the order of 15 ms. A fraction of the more viscous particles may
435 bounce from the vaporizer without detection. Non-refractory species in the particles that stick to
436 the vaporizer (such as OS and AS) are heated by heat transfer from the vaporizer surface. Some
437 species may evaporate in the form in which they are present in the particle, while others may
438 thermally decompose to other species, which then evaporate. For example, ammonium sulfate
439 may evaporate to $H_2SO_4(g)$ and $NH_3(g)$, but it may also thermally decompose to $SO_2(g)$, $SO_3(g)$
440 and $H_2O(g)$ (Hu et al., 2017b). Finally, these gaseous thermal decomposition products undergo
441 electron ionization to become positively charged species. Since the electrons used in EI have far
442 more energy (70 eV) than typical bonds in a molecule (~ 6 eV for S=O), the initial ions may
443 fragment into smaller ions if the ionization process results in absorption of > 6 eV of internal



444 energy by the molecule, beyond the ionization energy (Lambert, 1998). Some of the evaporated
445 $\text{H}_2\text{SO}_4(\text{g})$ may remain as H_2SO_4^+ after ionization, or it may fragment to HSO_3^+ or SO_x^+ ions.
446 $\text{SO}_2(\text{g})$ can only produce SO_x^+ ions. Thus the mixture of fragments observed will retain some
447 memory of the species that evaporated from the particles. If the mixture of evaporating species is
448 influenced by the particle composition (e.g. pH, AN, OA, or OS_p) then it may be possible to
449 calibrate the observed relationship to estimate a particle intensive chemical property.

450 Fig. 2A also shows a schematic close-up of the SV surface, which is the main point in the
451 instrument that controls ammonium sulfate fragmentation. In this diagram, we show a
452 non-smooth surface with pores, consistent with the fabrication of the vaporizer by sintering 50
453 μm tungsten spheres. The interaction of a particle with this porous surface is dependent on the
454 particle phase / viscosity. The red particles represent rigid (more solid-like) particles. These rigid
455 particles can simply bounce off of the vaporizer, leading to no detection. AS-dominated particles
456 are likely to be rigid (due to the solid phase of pure AS), thus increasing bounce and lowering the
457 AMS CE (Matthew et al., 2008; Middlebrook et al., 2012). AS particles can also become trapped
458 in the porous surface. When trapped, they are heated by conduction from the vaporizer surface
459 and by radiation from surrounding surfaces. They reach higher temperatures that lead to more
460 thermal decomposition, and a lower $\text{H}_2\text{SO}_4(\text{g})/\text{SO}_x(\text{g})$ ratio. In addition, molecules that evaporate
461 as $\text{H}_2\text{SO}_4(\text{g})$ from these trapped particles are likely to collide with tungsten surfaces on their way
462 out to the ionization region, leading to additional thermal decomposition (Hu et al., 2017b) and
463 further reducing the $\text{H}_2\text{SO}_4(\text{g})/\text{SO}_x(\text{g})$ ratio for the gases reaching the EI region, and thus the
464 $\text{H}_y\text{SO}_x^+/\text{SO}_x^+$ ion ratio.



465 The second case (blue particle) represents the situation where the particle is less
466 rigid/viscous or liquid. Acidic sulfate particles (with a lower fraction of the sulfate ions
467 neutralized by NH_4^+), particles with high AN_p , or particles coated with a large water or liquid
468 organic layer are more likely to deform upon impact and not bounce. This leads to an increased
469 CE (Matthew et al., 2008; Middlebrook et al., 2012; Hu et al., 2017a). There are several effects
470 that will lead to a higher $\text{H}_2\text{SO}_4(\text{g})/\text{SO}_x(\text{g})$ ratio reaching the ionization region in this situation:
471 (a) evaporated $\text{H}_2\text{SO}_4(\text{g})$ from particles that impact the front of the vaporizer and do not bounce
472 can now escape without further collisions with the tungsten surface; (b) the increased surface
473 area from impact deformation and the lower viscosity allow more $\text{H}_2\text{SO}_4(\text{g})$ molecules to escape
474 the particle before those molecules are heated to temperatures that would lead to thermal
475 decomposition.

476 In Fig. 2B, we show a conceptual model of the impact of these phenomena on the Chen
477 triangle. For very acidic sulfate (approx. $\text{pH} < 0$), the liquid character of the particles leads to
478 less bounce in the vaporizer. It also leads to faster evaporation, which reduces the internal
479 temperature for the particles and that of the evaporated molecules, leading to less fragmentation.
480 In this regime OS_f cannot be estimated, but pH may be, as long as it can be assumed (or shown
481 by additional measurements from the AMS or other instruments) that OS_f and non-volatile
482 cations are small. As an air mass becomes more neutralized by NH_4^+ , the particles become less
483 acidic and more rigid/viscous, leading to more thermal decomposition of the evaporated species,
484 and the fragmentation of ammonium sulfate occurs at the upper vertex of the triangle. In this
485 regime methods such as Chen et al. (2019) may be applicable to estimate OS_p , as long as there
486 are no other effects that interfere with the sulfate fragments detected (such as substantial



487 non-volatile cations or variations in possible OA effects). As more ammonia is added to an
488 air mass, the acidity of the particles decreases and the higher pH favors the partitioning of
489 $\text{HNO}_3(\text{g})$ to the particle phase, forming ammonium nitrate. If AN_f becomes high enough (> 0.3),
490 the particles again become less rigid/viscous and the fragmentation shifts again outside the Chen
491 triangle for the same reasons discussed for the acidic particles. Finally, Fig. 2C shows the
492 differences in the detection process and the fragments produced in the AMS for OS and/or
493 $\text{AS}/\text{H}_2\text{SO}_4$.

494

495 ***3.3 Evaluation of the Chen Method with Aircraft Field studies***

496 The results of applying the Chen et al. (2019) method to five aircraft campaigns are
497 shown in Fig. 1D. The effect of internally mixed ammonium nitrate (AN) was explored in Fig.
498 1A and Sect. 3.1 (for laboratory studies). Here we explore the effect for field data from
499 KORUS-AQ (near Seoul, South Korea) where AN was often a major aerosol component;
500 average $\text{AN}_f \sim 0.18$). As discussed in Sect. 3.1, as the percent of AN in laboratory mixtures of
501 AS/AN increases, so do the $n\text{fH}_y\text{SO}_x^+$ ions. The same effect is observed for the KORUS-AQ
502 campaign, although the departure from the AS vertex is observed at substantially lower AN
503 fractions for the field data ($\text{AN}_f \sim 0.30$). When field data is affected by AN, the Chen method
504 might be applicable for situations with $\text{AN}_f < 0.30$. At higher fractions, a correction could
505 potentially be developed, but with increased resulting uncertainty.

506 In Fig. 1D, average values for each campaign in less acidic ($\text{pH} > 0$) and lower AN_f ($<$
507 0.3) conditions are shown. In the absence of acidity, OS, or AN_f effects, it is expected that the
508 data would fall on top of the [1,1] pure AS point in the 1D triangle plot, but this is not observed.



509 This shift suggests that there are other factors (such as the presence of organics) that affect the
510 location of the pure AS point. In addition, the average values for the different campaigns vary
511 substantially, so it is unlikely that a “corrected” pure AS point can be used for all campaign
512 and/or lab data.

513 To further look into the potential effect of acidity, we consider the ATom campaigns in
514 Fig. 1C. ATom focused on remote oceanic air, with very low $AN_f (< 0.008)$. This is expected as
515 AN is semivolatile (DeCarlo et al., 2008; Hennigan et al., 2008; Nault et al., 2018) and for the
516 very low pH conditions during ATom (~ -1 to 1, average of -0.6), most of the nitrate will be in
517 the form of $HNO_3(g)$ (Guo et al., 2016). The PALMS instrument independently reports $OS_f \sim 0.3$
518 $- 0.7\%$ for ATom (depending on the pH). The results for ATom span the range between pure AS
519 and pure H_2SO_4 , following a monotonic trend as acidity increases, consistent with the laboratory
520 results and the results from the WINTER campaign in Chen et al. (2019). We hypothesize that
521 high acidity is leading to the observed departure from the Chen triangle. Hence, the ATom results
522 suggest that all of the sulfate sampled is inorganic and if the Chen method is applied $OS_f = -26\%$
523 to $+4\%$. Thus the Chen method is insufficient to describe the trends observed for very acidic
524 aerosols, until pH increases to ~ 0 (where the ATom data starts to converge onto the pure AS data
525 point). For campaigns containing particles of $pH > 0$, the Chen method might be applicable.

526 To further illustrate that the ATom and KORUS-AQ campaigns are representative of the
527 range of airmasses in the troposphere, Fig. 1D shows results for two additional campaigns that
528 focused on the continental US. SEAC⁴RS and WINTER represent chemical regimes that are not
529 extremely acidic (average pH SEAC⁴RS ~ -0.2 , WINTER pH ~ 1.2). SEAC⁴RS had low $AN_f (\sim$
530 $0.04)$, while WINTER had high $AN_f (\sim 0.25)$. It is observed that every single campaign average



531 falls outside of the triangle (for the full campaign and non-acidic, low AN_f averages), indicating
532 that the Chen et al. method, as proposed, breaks down for many regions of the atmosphere.

533 Average AN_p , OA_p , and pH values for different campaigns are shown in table S1.

534

535 **3.4 Specification of aerosol chemical regimes for feasibility of OS_f quantification**

536 In Fig. 3A, we introduce a plot of AN_f vs. pH that can be used to evaluate the
537 applicability of the OS_f methods to different datasets. Data for five different campaigns (those
538 with AS calibrations, labelled “C” in Table 1) are shown, along with the campaign averages.

539 Regime I (“highly acidic, low AN_f ”) occupies the bottom left quadrant, where $AN_f < 0.3$ and pH
540 < 0 . Campaigns sampling the more remote atmosphere (e.g. ATom-1, 89% of datapoints;
541 ATom-2, 80%), and a fraction of the data from continental campaigns (SEAC⁴RS, 13% ; DC3 ,
542 40%) fall in this regime. For remote regions, emissions (such as NH_3 and NO_x) are generally low.
543 Remote oceanic regions are relatively isolated from the major continental ammonia sources
544 (Paulot et al., 2015). Therefore, less ammonia is available to balance the hydronium ions from
545 H_2SO_4 , leading to high acidity (Quinn et al., 1988; Keene, 2002; Nault et al., 2020). Highly
546 acidic aerosols and lack of NH_3 shift HNO_3 to the gas phase, so low AN_f is observed. In contrast,
547 for sampling in polluted source regions with strong HNO_3 formation and substantial NH_3
548 emissions, a much smaller fraction of the data falls in this regime (e.g. only 4% for
549 KORUS-AQ). In Sect. 3.5 we discuss the potential to estimate pH from AMS data in regime I.

550 Regime II (lower right) involves less acidic conditions (pH > 0) and lower AN_f (< 0.3). In
551 this region sulfate fragmentation in the AMS is not strongly impacted by either AN_f or acidity. In
552 principle, in this regime the recently proposed sulfate deconvolution methods can be used. The



553 geographical regions studied in Chen et al. (2019) and Song et al. (2019) generally fall in this
554 regime, and this explains the lack of large negative OS_f values in those studies, in contrast to our
555 observations for other regions. About half of our campaign data is located in this regime, more
556 so for the continental campaigns and much less for the remote campaigns. Specifically, 65% of
557 KORUS-AQ, 60% of DC3, 87% of SEAC⁴RS, 11% of ATom-1 and 20% of ATom-2 fall in this
558 regime. We have applied the 1D version of the Chen method to each field campaign after
559 filtering it by the AN_f and pH constraints for regime II. OS_f is nominally slightly greater than
560 zero for ATom-1 ($OS_f \sim 3\%$, greater than the 0.3% estimate in regime II from PALMS (for
561 ATom-1 and ATom-2, estimated by only considering the sulfate moiety from the IEPOX or
562 glycolic acid sulfate (GAS) OS, neither of which was detected in the supermicron aerosol (Froyd
563 et al., 2009, 2019; Liao et al., 2015)) but still small, (see Fig. S7) much less than zero for
564 ATom-2 ($OS_f \sim -23\%$) and KORUS-AQ ($OS_f \sim -26\%$). This shows that even when pH and AN
565 are not major influences on the sulfate fragmentation, estimating OS with sulfate ions may be
566 susceptible to inaccuracies in AS calibrations, noise present in the ambient data, or other factors.

567 We also show results from applying the Song et al. (2019) method in regime II (which is
568 based on similar principles to the Chen method) in Fig. S8. Similarly to the Chen method, we see
569 that most OS_f values are predicted to be less than zero. For the entire atmosphere, shown in Fig.
570 S9, the distribution for % OS looks similar to Fig. S8.

571 Regime III is characterized by high AN_f (> 0.3) and lower acidity ($pH > 0$). This
572 chemical regime primarily exists in polluted continental regions near large source regions such
573 as megacities and agricultural regions, as high NO_x and NH_3 emissions can lead to increased
574 particulate AN and an increase in aerosol pH (Pye et al., 2019). In this regime, there are strong



575 variations in the AMS sulfate fragments that are driven by AN_f . OS_f cannot be estimated with the
576 AMS sulfate fragmentation methods proposed so far, unless they are further modified to account
577 for the AN_f effect. ~ 31% of KORUS-AQ data falls in this regime, but almost none of the data
578 from the rural / remote campaigns falls in this region, as AN typically evaporates as the air is
579 diluted during advection away from polluted regions (DeCarlo et al., 2008).

580 Finally, regime IV in the top left quadrant has high AN ($AN_f > 0.3$) and high acidity (pH
581 < 0). This chemical regime is unlikely to be observed in the real atmosphere, and indeed there
582 are very few points in that region for our campaigns. Sulfate is ubiquitous (Zhang et al., 2007b;
583 Hodzic et al., 2020), and nitrate is not thermodynamically stable in the aerosol phase together
584 with acidic sulfate for $pH < 0$ (Guo et. al., 2016). For all campaigns we observe ~ 0% of points
585 occupying this regime. Very unusual datapoints can be observed when ammonium
586 nitrate-containing particles are externally mixed with acidic sulfate containing particles in an
587 air mass.

588 Since the field studies analyzed here targeted large regions but did not sample many
589 others, it is of interest to evaluate the fraction of the troposphere located in each one of the
590 chemical regimes. The results of the GEOS-Chem v12 model are used for this purpose in Fig. 3B
591 and shown as a global map in Fig. 4 and Fig. S10. ~ 67% of the model troposphere exists in
592 regime I ($pH < 0$). In addition, ~ 33% of the global troposphere exists in regime II where it may
593 be feasible to estimate OS_f from AMS fragments. Less than 1% of the modeled atmosphere
594 exists in regime III (upper right quadrant) where ammonium nitrate strongly influences sulfate
595 fragmentation, consistent with the relatively small very polluted geographical regions with very
596 large AN_f . Finally, none of the data fell in regime IV, consistent with aerosols being assumed to



597 be internally mixed in GEOS-Chem. At the surface during December, January, and February
598 (DJF) (Fig. 4A), most of the remote oceans fall in regime I ($\text{pH} < 0$ and $\text{AN}_f < 0.3$), while regime
599 II ($\text{pH} > 0$ and $\text{AN}_f < 0.3$) is dominant over continental regions. At the surface in June, July, and
600 August (JJA) (Fig. 4C), most of the globe is in regime II. Very little of the data falls in regime
601 III, except parts of Asia, regardless of season. A similar pattern is observed in the free
602 troposphere (Fig. 4B and 4D) with some geographical differences. Regime III ($\text{pH} > 0$ and $\text{AN}_f >$
603 0.3), which represents pollution hotspots, is observed in a large region in Asia during the
604 Summer months, whereas the Winter months are dominated by regime I (low pH). The Summer
605 months in the free troposphere are also mostly in regime II, especially over continental regions.
606 Due to averaging of an entire year, as well as the limited spatial resolution of the GEOS-Chem
607 model, locations and periods of high AN_f hotspots are not as prominent in these results, even
608 when the data is divided by season.

609

610 **3.5 Potential pH estimation from AMS measurements**

611 **3.5.1 Estimation of pH from AMS sulfate fragments**

612 In Sect. 3.4, we introduced chemical regime I with low pH and low AN_f . In this regime,
613 which encompasses about half of the campaign data and $\frac{2}{3}$ of the modeled global troposphere,
614 PALMS data shows that the overwhelming majority of the sulfate is inorganic, with OS_f
615 contributing $\sim 0.7\%$ to total sulfate by mass during ATom-1 and ATom-2 when $\text{pH} < 0$ (see Fig.
616 S7, in regime I). This removes sulfate fragmentation changes caused by AN and sulfate type (OS
617 vs. AS), indicating that sulfate fragmentation is almost exclusively controlled by the acidity of
618 the aerosol. Fig. 1C shows that $f\text{H}_2\text{SO}_4^+$ and $f\text{HSO}_3^+$, i.e. the amount of sulfate fragments



619 retaining one or two hydrogens ($H_2SO_4^+$ and HSO_3^+) relative to the sulfate fragments without a
620 hydrogen atom (SO_3^+ , SO_2^+ , SO^+) increases as pH decreases.

621 In Fig. 5 we show the relationship between $H_ySO_x^+/SO_x^+$ and aerosol pH. As the
622 relationship is noisy for individual data points, we show the results for 5% quantiles of the data.
623 $H_ySO_x^+/SO_x^+$ appears to show a proportional relationship with decreasing pH for the ATom
624 campaigns, for which much of the data is in regime I. The KORUS-AQ data, of which very little
625 falls in the regime I, does not show a relationship between these variables, as expected. A fitted
626 equation to the ATom relationship may allow the real-time estimation of pH for different air
627 masses for campaigns in regime I as:

$$pH = -1.3 (\pm 0.06) + 6.0 (\pm 1.2) \times e^{-1.3 (\pm 0.18) \times \frac{H_ySO_x^+}{SO_x^+}} \quad \text{Eq. 13}$$

628
629 As shown in the histogram in Fig. 5B, this relationship is applicable to a substantial fraction of
630 ambient observations. This estimation equation likely needs to be calibrated for each instrument
631 (e.g. by sampling sulfate particles with different acidities), since the sulfate fragmentation does
632 vary with instrument (Chen et al., 2019) (and potentially also in time for a given instrument).

633 Although an estimation equation that apparently works for only one unit of pH may seem
634 of limited value, two caveats apply: first, it is of high value to know that $pH < 0$ for a certain air
635 mass (as opposed to e.g. $pH = 2$ or 3 that are frequently encountered). Second, the range of pH
636 below 0 is limited here due to not considering the activity coefficient. If that coefficient was
637 included, the predicted pH range in this regime would be ~ -4 to 0.

638

639 **3.5.2 Estimation of pH from Ammonium Balance**



640 Ammonium balance (NH_{4_bal}) (Eq. (7)) is often used as a qualitative indicator of acidity.
641 (Zhang et al., 2007a) showed that pH under constant temperature and RH was well correlated
642 with ammonium balance, but much more scatter was observed when the instantaneous T and RH
643 were used. Several studies have argued that ammonium balance cannot be used to estimate
644 ambient pH (e.g., (Guo et al., 2015, 2016; Hennigan et al., 2015; Weber et al., 2016); however,
645 those studies were all performed at continental ground sites that were in the less-acidic chemical
646 regimes (II and III), and where daily temperature and humidity changes were strong. As shown
647 in Fig. 6, NH_{4_bal} and pH for the aircraft studies show a strong and consistent relationship in
648 regime I ($pH < 0$), providing another potential method for estimating pH. As ammonium balance
649 increases, so does pH across the six campaigns studied. These data are generally outside of the
650 continental boundary layer, where temperature and RH change less in a diurnal cycle, reducing
651 the impact of those changes on pH. For data in regimes II-III ($pH > 0$) some proportionality of
652 pH and NH_{4_bal} is still observed on average, but with more dispersion across campaigns. Given
653 the similarity of the results for regime I, the fitting equation of pH vs. ammonium balance may
654 be used to provide a near real-time estimate of pH (for $NH_{4_bal} < 0.65$).

$$pH = -1.1(\pm 0.031) + 1.7(\pm 0.089) * NH_{4_bal} \quad \text{Eq. 14}$$

655

656 As shown in the histogram in Fig 6B-6D, this relationship is also applicable to a
657 substantial fraction of ambient regions. This estimation equation should be tested with other
658 studies. An advantage of this relationship (vs. the one based on $H_ySO_x^+ / SO_x^+$) is that it is likely to
659 be less instrument-dependent, as long as careful calibrations of RIE_{NH_4} and RIE_{SO_4} have been
660 performed. Conditions where non-volatile cations (e.g. Na^+ , K^+ , Ca^{2+}) are important for



661 submicron particles could lead to deviations from this relationship (Guo et al., 2020). However,
662 such conditions are infrequent in remote air (Nault et al., 2020) and can be diagnosed by
663 concurrent supermicron or filter measurements.

664

665 3.5.3 Application of pH estimation methods to ambient data

666 As discussed above, ammonium balance and $\text{H}_y\text{SO}_x^+/\text{SO}_x^+$ are two measurements that
667 may be used to estimate aerosol acidity in parts of the atmosphere. In Fig. 7 these two methods
668 are applied to one flight during ATom-1 and an SO_2 plume sampled during WINTER. In Fig. 7A,
669 both $\text{H}_y\text{SO}_x^+/\text{SO}_x^+$ and NH_{4_bal} follow the trend for E-AIM calculated pH during most periods
670 when $\text{pH} < 0$, even at one minute time resolution.

671 As expected from Fig. 6, NH_{4_bal} is a less noisy, more robust metric for estimating pH at
672 one minute time resolution. Unlike $\text{H}_y\text{SO}_x^+/\text{SO}_x^+$, NH_{4_bal} appears to be able to capture basic pH
673 trends at the full range of pH values observed during this flight in ATom-1. NH_{4_bal} also matches
674 the E-AIM predicted pH well for the WINTER power plant plume. For RF01 in ATom-1
675 (WINTER), NH_{4_bal} predicted pH has an $R^2 \sim 0.6$ (0.9) for $\text{pH} < 0$ (Fig. 7C-D). This shows that in
676 the remote atmosphere (like in ATom) or in an SO_2 plume, NH_{4_bal} has the potential to allow fast
677 estimation of pH, even under relatively low sulfate concentrations, albeit not perfectly. More
678 scatter is observed for the estimate based on $\text{H}_y\text{SO}_x^+/\text{SO}_x^+$, indicating that longer averages are
679 needed for this method. The error is typically within ± 0.5 pH units, which is thought to be the
680 accuracy of thermodynamic pH estimation models.

681

682 3.6 Possibility of Estimating CE from Sulfate Fragmentation



683 From the previous discussion it is clear that sulfate fragmentation changes due to some of
684 the same factors (acidity, AN_f) that influence ambient AMS CE. It is of interest to explore
685 whether a quantitative estimate of ambient particle CE could be derived from the measured
686 sulfate fragments, at least under some conditions, as it could provide a complementary
687 characterization to the CE estimates from the Middlebrook et al. (2012) parameterization. In Fig.
688 8 we show the CE estimated from Middlebrook et al. (2012) vs. $H_ySO_x^+/SO_x^+$ for ATom and
689 KORUS-AQ. CE does show some relationship with $H_ySO_x^+/SO_x^+$, with most sensitivity around
690 $CE \sim 0.8-0.9$. A substantial level of noise is observed on the high-time resolution data, and the
691 trend varies between the two campaigns (where variations in CE are controlled by two different
692 effects, acidity vs AN_f). Further research would be necessary to evaluate whether this method
693 could be used to estimate CE.

694

695 Conclusions

696 The presence of organosulfates in particles is a topic of much recent interest, but there is
697 a lack of online methods to quantify them. Two methods have been proposed to use widely
698 available AMS data to quantify OS_f (Chen et al., 2019; Song et al., 2019). However, these
699 methods have only been applied to ground continental datasets, to our knowledge. We show
700 using both laboratory and field data that both high acidity (chemical regime I in this work) and
701 high AN_f (regime III) result in major changes in sulfate fragmentation, which often produce
702 nonsensical results for the OS_f methods. Regime I accounts for $\sim 2/3$ of the global troposphere,
703 while regime III can be important in polluted regions (e.g. Seoul region), and thus it is critical to
704 avoid applying the proposed OS_f estimation methods in these regimes. In regime II, with lower



705 acidity and lower nitrate ($\text{pH} > 0$, $\text{AN}_f < 0.3$) OS_f estimation methods may be applicable, if no
706 other effects (e.g. significant non-volatile cations or variations in OA effects) confound the
707 sulfate fragmentation. For reasons not fully understood, fragmentation of the sulfate ions in the
708 lab vs. ambient data differ at times.

709 We investigated two different methods to estimate pH in real-time in regime I ($\text{pH} < 0$
710 and $\text{AN}_f < 0.3$), based on the AMS $\text{H}_y\text{SO}_x^+/\text{SO}_x^+$ fragment ratio and the ammonium balance,
711 respectively, without the need to run a thermodynamic model, and without the need for gas-phase
712 NH_3 or HNO_3 measurements. Low OS_f and non-volatile cations need to be assumed or confirmed
713 from AMS and other measurements. The ammonium balance method shows better performance.
714 These *in-situ* and direct pH estimation methods should be applicable in the remote atmosphere
715 (oceanic regions, and often the continental free troposphere when not recently impacted by
716 surface sources). Both the OS_f and pH estimations require careful instrument calibration for a
717 given campaign, and the methods based on sulfate fragments are expected to be
718 instrument-dependent, including for the same instrument in time when filaments or the vaporizer
719 are replaced, or when the instrument is re-tuned. Both methods should be further evaluated with
720 data from other studies.

721 We propose a conceptual model to explain the observed sulfate fragmentation changes
722 with changing particle chemical composition. As particles become more acidic or higher in AN,
723 a higher fraction of $\text{H}_2\text{SO}_4(\text{g})$ can reach the ionization region, leading to changes in the observed
724 ion population. Since AMS CE is thought to be controlled by the same effects, we explore
725 whether it can be estimated from the observed sulfate fragmentation, and find that while changes
726 in $\text{H}_y\text{SO}_x^+/\text{SO}_x^+$ do correlate to changes in CE, the relationship is not the same across different



727 campaigns. Further investigation of this relationship, especially when direct CE measurements
728 are available via internal AMS light scattering, would be of interest.

729

730 **Acknowledgements**

731 This work was supported by NASA grants NNX15AH33A & 80NSSC19K0124, and a CIRES
732 IRP project. We thank the members of the Jimenez group, the AMS users community, Weiwei
733 Hu, Amber Ortega, and Patrick Hayes for help with data acquisition during SEAC⁴RS and DC-3;
734 Jason St. Clair, Alex Teng, Michelle Kim, John Crouse, and Paul Wennberg for providing
735 CIT-CIMS HNO₃ data; Joel Thornton, Felipe Lopez-Hilfiker, and Ben Lee for providing
736 UW-CIMS HNO₃ data during WINTER; Karl Froyd, Gregory P. Schill, and Daniel Murphy for
737 providing PALMS organosulfate data for ATom campaigns; and Glenn Diskin for providing
738 DLH H₂O data.
739

740 **Data Availability**

741 DC3 data available at [DOI: 10.5067/Aircraft/DC3/DC8/Aerosol-TraceGas](https://doi.org/10.5067/Aircraft/DC3/DC8/Aerosol-TraceGas), last accessed on 9
742 September, 2018. SEAC⁴RS data available at
743 <http://doi.org/10.5067/Aircraft/SEAC4RS/Aerosol-TraceGas-Cloud>, last accessed on 27 April,
744 2020. WINTER data available at https://data.eol.ucar.edu/master_lists/generated/winter/, last
745 accessed 27 April 2020. KORUS-AQ data available at [DOI:](https://doi.org/10.5067/Suborbital/KORUSAQ/DATA01)
746 [10.5067/Suborbital/KORUSAQ/DATA01](https://doi.org/10.5067/Suborbital/KORUSAQ/DATA01), last accessed 14 June, 2018. ATom-1 and ATom-2
747 data available at <https://doi.org/10.3334/ORNLDAAAC/158>, last accessed 27 April 2020.



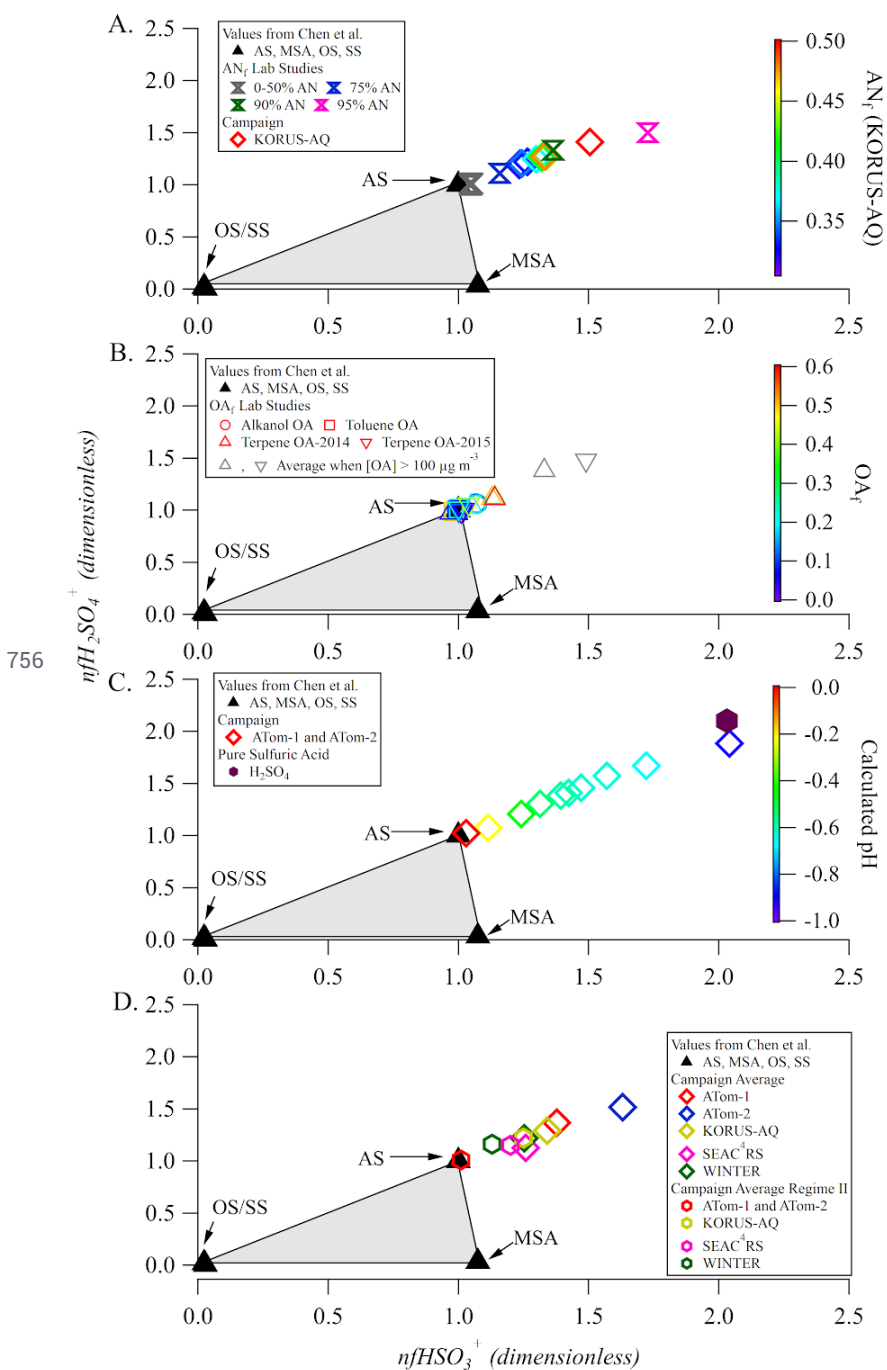
748 **Tables**

749 *Table 1. Summary of the campaigns used in this study. See SI Fig. S1 for flight paths. Reference*
 750 *label refers to the type of data used for each campaign throughout this paper, depending on the*
 751 *quality and completeness of the data, for the purposes of a specific analysis. A : ammonium*
 752 *balance, f: SO₄ campaign-averaged fragments, F: SO₄ campaign-average and time-resolved*
 753 *fragments , and C: pure AS calibration data reliable and used.*

Campaign	Location	Season/Year	References	Reference Label
DC3: Deep Convective Clouds and Chemistry	Mid-Latitude Continental United States	May-June 2012	Barth et al. , 2015	A
SEAC ⁴ RS: Studies of Emissions and Atmospheric Composition, Clouds and Climate Coupling by Regional Surveys	Continental United States	Summer 2013	Wagner et al., 2015; Toon et al., 2016	A, f, C
WINTER: Wintertime Investigation of Transport, Emissions, and Reactivity	Eastern United States, continental and marine	Winter 2015	Schroder et al., 2018; Shah et al., 2018	A, f, C
KORUS-AQ: Korean United States Air Quality	South Korean Peninsula and Yellow Sea	Spring 2016	Nault et al., 2018	A, F, C
ATom-1: Atmospheric Tomography Mission 1	Remote Pacific and Atlantic Basins	Boreal Summer 2016	Hodzic et al., 2020; Brock et al., 2019; Hodshire et al., 2019	A, F, C
ATom-2: Atmospheric Tomography Mission 2	Remote Pacific and Atlantic Basins	Boreal Winter 2017	Hodzic et al., 2020	A, F, C

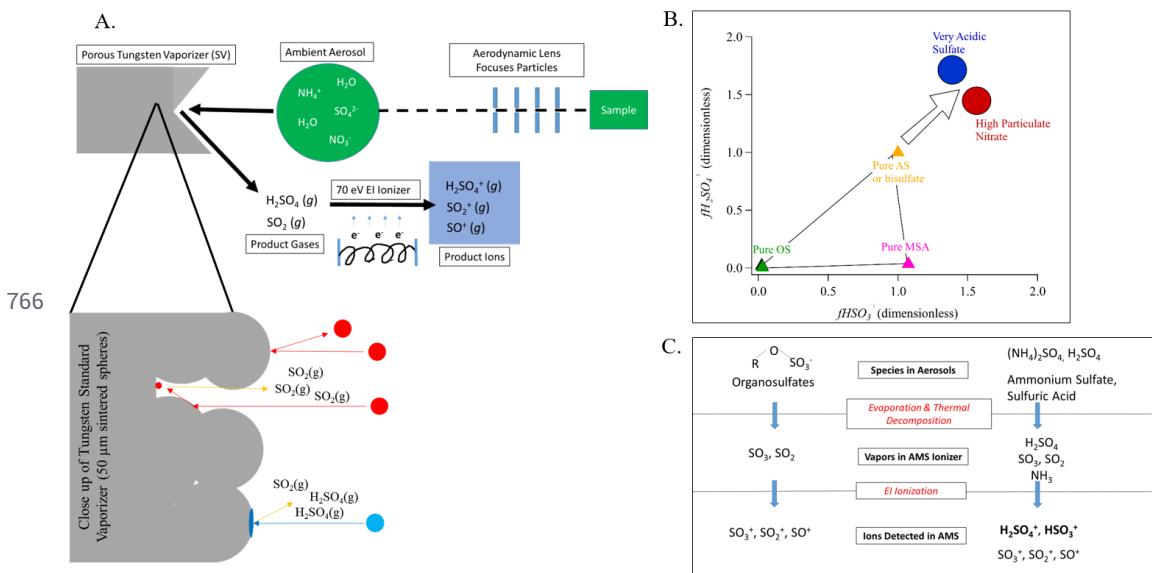
754

755

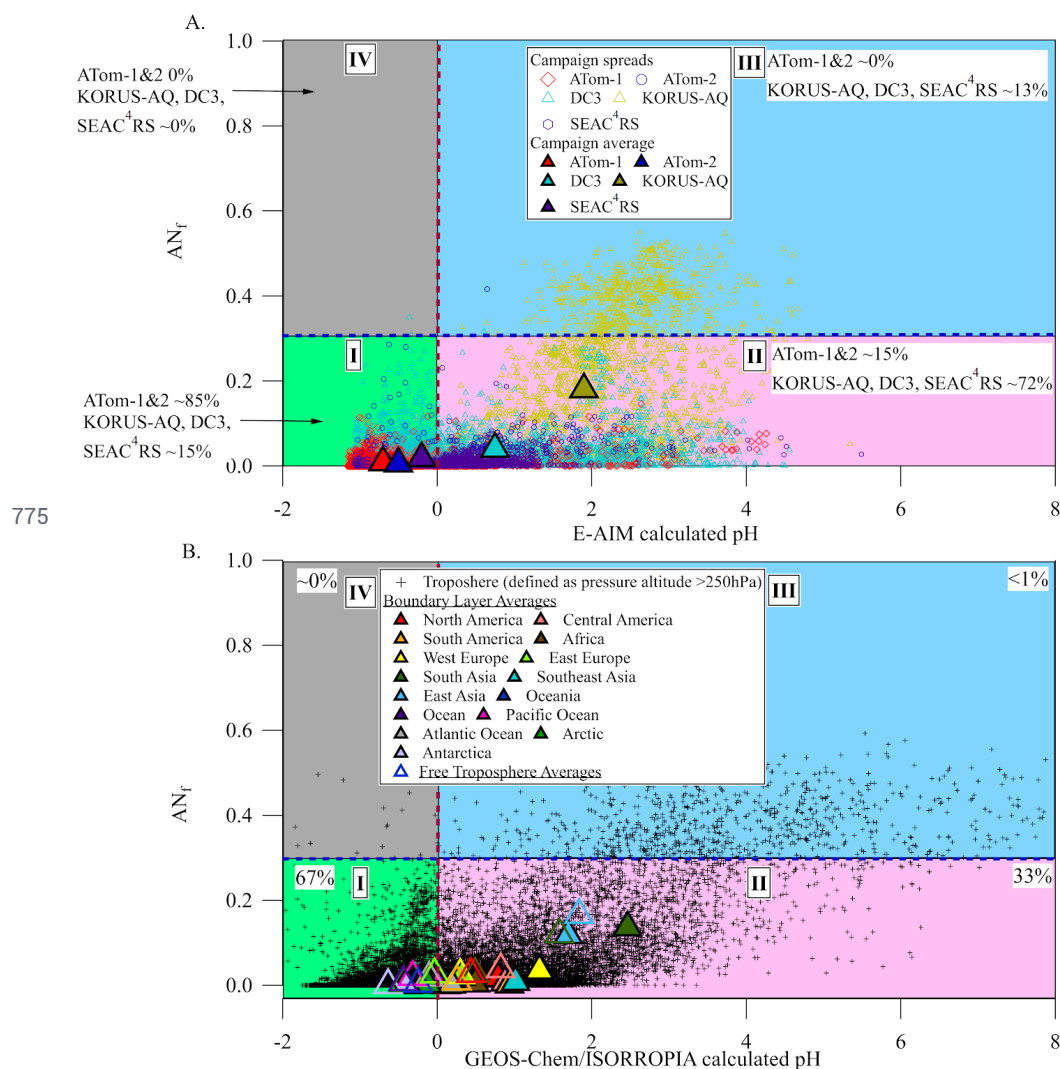




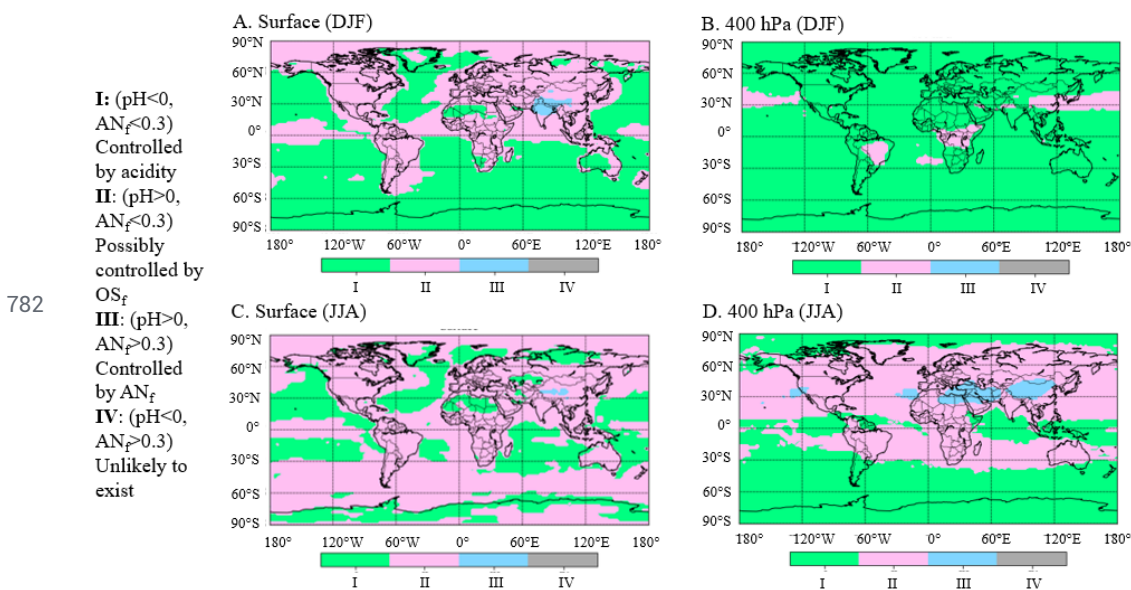
757 Fig. 1. Laboratory and field data for sulfate fragmentation shown in the triangle diagram
758 proposed by Chen et al. (2019). (A) Data split into 10 quantiles of AN_f value for the full
759 KORUS-AQ campaign, as well as for different laboratory internal mixtures of AS and AN. (B)
760 Data from two chamber experiments, split into 5 quantiles of OA_f . Data with very high OA
761 ($>100 \mu\text{g m}^{-3}$) are shown as grey triangles. Two separate datasets of monoterpene SOA chamber
762 experiments are labelled as “2014” and “2015”. (C) Data split into 10 quantiles by pH for
763 ATom-1 and 2, colored by pH from E-AIM. (D) Averages for 5 aircraft campaigns for the full
764 campaign and a subset of each campaign where $\text{pH} < 0$ and $AN_f < 0.3$.
765



767 Fig. 2. (A) Simplified schematic of the AMS detection process, including a close up of the
 768 tungsten standard vaporizer surface and the different species produced by AS and OS. (B)
 769 Conceptual model of the position of particles of different compositions in the Chen et al. (2019)
 770 triangle plot. As particles become more acidic or higher in particulate nitrate, the ratio of the
 771 AMS hydrogenated to total sulfate fragments increases. When sulfate is present as AS (or
 772 mixtures of AS and ammonium bisulfate), the sulfate fragmentation is mainly impacted by OS
 773 vs. AS vs. MSA relative concentrations inside the Chen triangle. (C) Schematic of the
 774 transformations during the AMS detection process for OS and AS.



776 Fig. 3. (A) location of the aircraft campaign 1-minute data points on the chemical regimes
 777 defined in this paper (AN_r , from AMS measurements) vs. E-AIM pH. SEAC⁴RS, WINTER, and
 778 KORUS-AQ are averaged to one value, for brevity, but defined individually in Sect. 3.4. (B)
 779 Location of global GEOS-Chem v12 results in the chemical-regimes diagram. Yearlong averages
 780 shown as large triangles.
 781



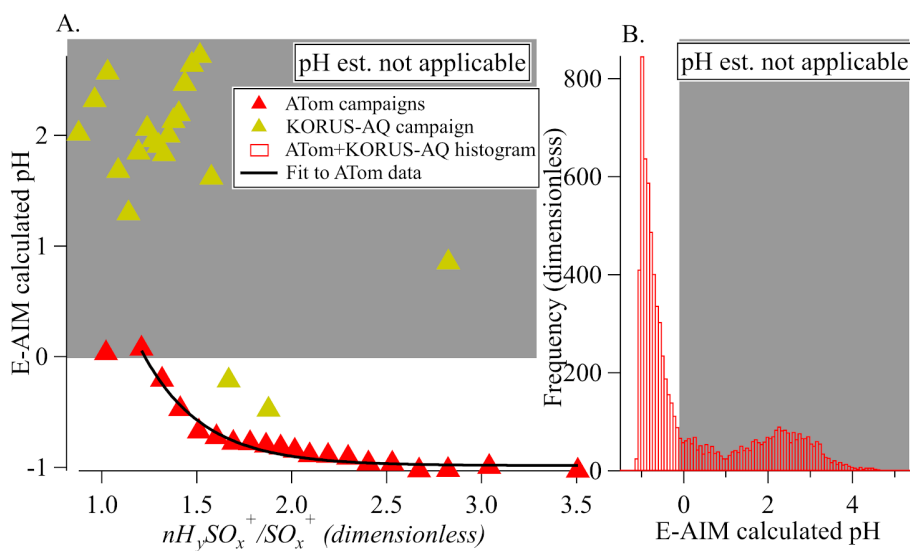
783 Fig. 4. Areas characterized by different chemical regimes according to results from
784 GEOS-Chem v12. (A) Surface for December, January, and February (DJF), (B) 400 hPa for DJF,
785 (C) Surface for June, July, and August (JJA), (D) 400 hPa for JJA. Roman numerals correspond
786 to regimes in Fig. 3.

787

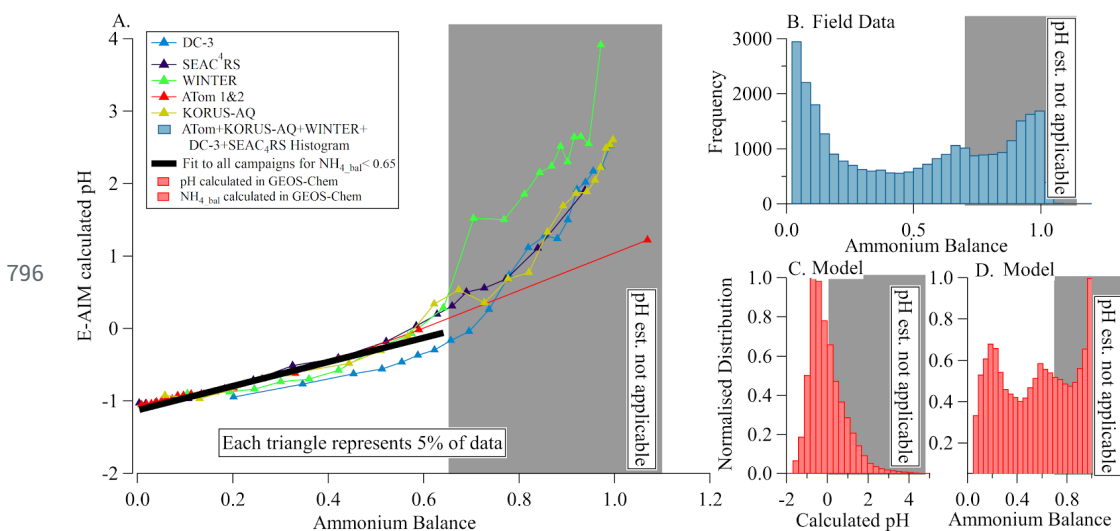


788

789



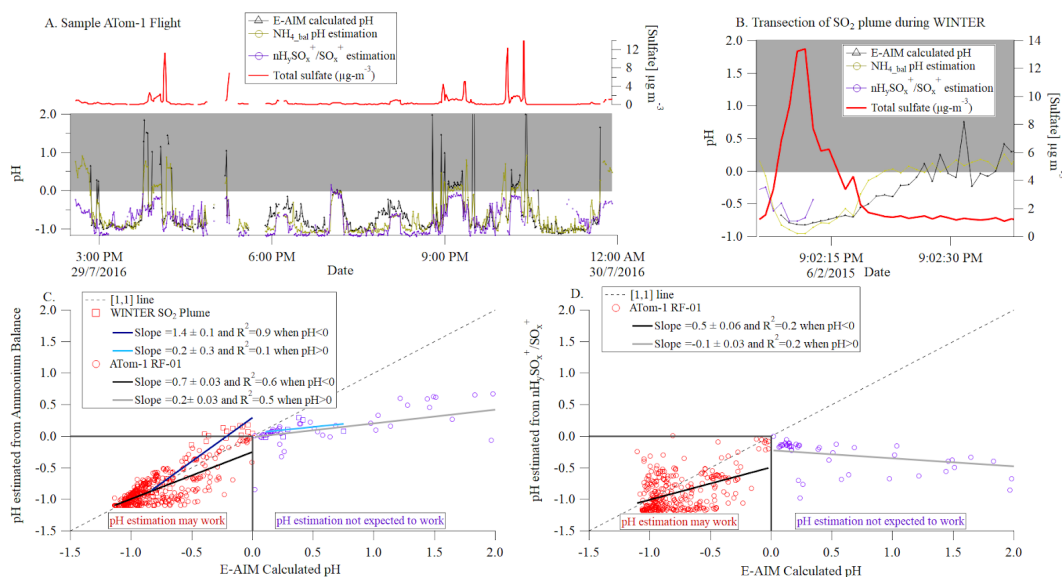
790 Fig. 5. (A) pH vs. sulfate fragmentation indicator ($H_ySO_x^+/SO_x^+$) for the ATom and KORUS-AQ
791 campaigns, and binned by $nH_ySO_x^+/SO_x^+$. The black line is an exponential fit to ATom data (see
792 text). (B) histogram of the calculated pH for the 1-minute datapoints from the ATom-1,2 and
793 KORUS-AQ datasets. In both panels, the white (gray) area shows the regime where pH can
794 (cannot) be estimated from the sulfate fragmentation.
795



797 Fig 6. (A) calculated pH vs. ammonium balance for multiple campaigns. Quantiles of the data
798 are used to reduce the impact of noise. The black line is an orthogonal distance regression (ODR)
799 fit to the campaign data for values with $\text{NH}_{4_Bal} < 0.65$. B) Histogram of measured ammonium
800 balance for the 6 campaigns. (C) and (D), pH and ammonium balance from GEOS-Chem (pH
801 calculated with ISORROPIA). In all panels the white (grey) areas encompass the data points for
802 which pH can (cannot) be estimated from the measured ammonium balance.
803

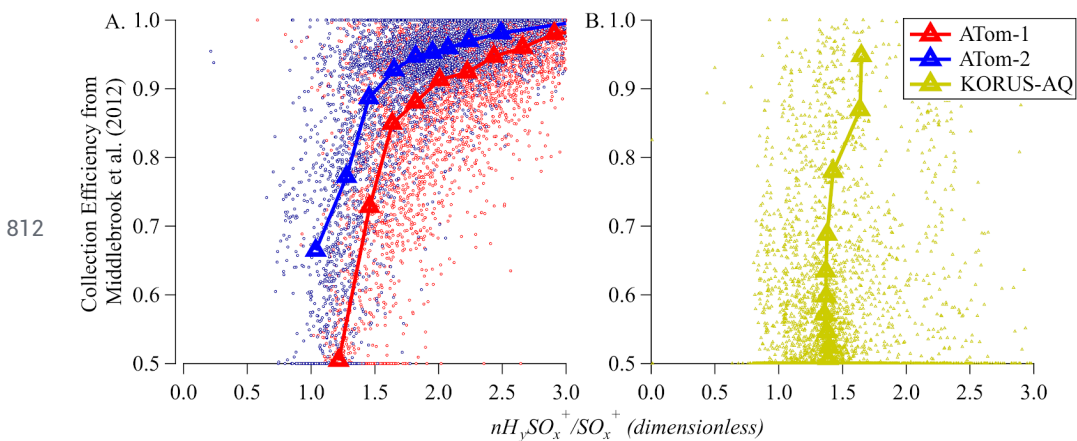


804



805

806 Fig. 7. (A) Time series of sulfate, pH calculated from E-AIM and estimated from $\text{H}_y\text{SO}_x^+/\text{SO}_x^+$,
 807 and NH_{4_Bal} for one flight during ATom-1 (at 1 min. resolution, filtered to remove points where
 808 sulfate was less than 3 times its detection limit). (B) Time series of sulfate and pH for a large
 809 power plant plume sampled during WINTER. (C) Scatterplot of pH predicted from NH_{4_Bal} vs.
 810 E-AIM pH for the data above. (D) Scatterplot of pH predicted from $\text{H}_y\text{SO}_x^+/\text{SO}_x^+$ vs. E-AIM pH
 811 for the ATom flight.





816

817 References

- 818 Ackendorf, J. M., Ippolito, M. G. and Galloway, M. M.: pH Dependence of the
819 Imidazole-2-carboxaldehyde Hydration Equilibrium: Implications for Atmospheric Light
820 Absorbance, *Environ. Sci. Technol. Lett.*, 4(12), 551–555, doi:10.1021/acs.estlett.7b00486,
821 2017.
- 822 Alfara, M. R., Coe, H., Allan, J. D., Bower, K. N., Boudries, H., Canagaratna, M. R., Jimenez, J.
823 L., Jayne, J. T., Garforth, A. A., Li, S.-M. and Worsnop, D. R.: Characterization of urban and
824 rural organic particulate in the Lower Fraser Valley using two Aerodyne Aerosol Mass
825 Spectrometers, *Atmos. Environ.*, 38(34), 5745–5758, doi:10.1016/j.atmosenv.2004.01.054, 2004.
- 826 Anon: Atmospheric chemistry and physics: from air pollution to climate change, *Choice*
827 *Reviews Online*, 44(08), 44–4512–44–4512, doi:10.5860/CHOICE.44-4512, 2007.
- 828 Bahreini, R., Dunlea, E. J., Matthew, B. M., Simons, C., Docherty, K. S., DeCarlo, P. F., Jimenez,
829 J. L., Brock, C. A. and Middlebrook, A. M.: Design and Operation of a Pressure-Controlled Inlet
830 for Airborne Sampling with an Aerodynamic Aerosol Lens, *Aerosol Sci. Technol.*, 42(6),
831 465–471, doi:10.1080/02786820802178514, 2008.
- 832 Bahreini, R., Ervens, B., Middlebrook, A. M., Warneke, C., de Gouw, J. A., DeCarlo, P. F.,
833 Jimenez, J. L., Brock, C. A., Neuman, J. A., Ryerson, T. B., Stark, H., Atlas, E., Brioude, J.,
834 Fried, A., Holloway, J. S., Peischl, J., Richter, D., Walega, J., Weibring, P., Wollny, A. G. and
835 Fehsenfeld, F. C.: Organic aerosol formation in urban and industrial plumes near Houston and
836 Dallas, Texas, *J. Geophys. Res.*, 114, 1185, doi:10.1029/2008JD011493, 2009.
- 837 Barth, M. C., Cantrell, C. A., Brune, W. H., Rutledge, S. A., Crawford, J. H., Huntrieser, H.,
838 Carey, L. D., MacGorman, D., Weisman, M., Pickering, K. E., Bruning, E., Anderson, B., Apel,
839 E., Biggerstaff, M., Campos, T., Campuzano-Jost, P., Cohen, R., Crouse, J., Day, D. A., Diskin,
840 G., Flocke, F., Fried, A., Garland, C., Heikes, B., Honomichl, S., Hornbrook, R., Huey, L. G.,
841 Jimenez, J. L., Lang, T., Lichtenstern, M., Mikoviny, T., Nault, B., O’Sullivan, D., Pan, L. L.,
842 Peischl, J., Pollack, I., Richter, D., Riemer, D., Ryerson, T., Schlager, H., St. Clair, J., Walega, J.,
843 Weibring, P., Weinheimer, A., Wennberg, P., Wisthaler, A., Wooldridge, P. J. and Ziegler, C.: The
844 Deep Convective Clouds and Chemistry (DC3) Field Campaign, *Bull. Am. Meteorol. Soc.*,
845 96(8), 1281–1309, doi:10.1175/BAMS-D-13-00290.1, 2015.
- 846 Bertram, T. H. and Thornton, J. A.: Toward a general parameterization of N_2O_5 reactivity on
847 aqueous particles: the competing effects of particle liquid water, nitrate and chloride, *Atmos.*
848 *Chem. Phys.*, 9(21), 8351–8363, 2009.
- 849 Bey, I., Jacob, D. J., Yantosca, R. M., Logan, J. A., Field, B. D., Fiore, A. M., Li, Q., Liu, H. Y.,
850 Mickley, L. J. and Schultz, M. G.: Global modeling of tropospheric chemistry with assimilated
851 meteorology: Model description and evaluation, *J. Geophys. Res.*, 106(D19), 23073–23095,
852 doi:10.1029/2001JD000807, 2001.



- 853 Canagaratna, M. R., Jayne, J. T., Jimenez, J. L., Allan, J. D., Alfarra, M. R., Zhang, Q., Onasch,
854 T. B., Drewnick, F., Coe, H., Middlebrook, A., Delia, A., Williams, L. R., Trimborn, A. M.,
855 Northway, M. J., DeCarlo, P. F., Kolb, C. E., Davidovits, P. and Worsnop, D. R.: Chemical and
856 microphysical characterization of ambient aerosols with the aerodyne aerosol mass spectrometer,
857 *Mass Spectrom. Rev.*, 26(2), 185–222, doi:10.1002/mas.20115, 2007.
- 858 Carlton, A. G., de Gouw, J., Jimenez, J. L., Ambrose, J. L., Attwood, A. R., Brown, S., Baker, K.
859 R., Brock, C., Cohen, R. C., Edgerton, S., Farkas, C. M., Farmer, D., Goldstein, A. H., Gratz, L.,
860 Guenther, A., Hunt, S., Jaeglé, L., Jaffe, D. A., Mak, J., McClure, C., Nenes, A., Nguyen, T. K.,
861 Pierce, J. R., de Sa, S., Selin, N. E., Shah, V., Shaw, S., Shepson, P. B., Song, S., Stutz, J.,
862 Surratt, J. D., Turpin, B. J., Warneke, C., Washenfelder, R. A., Wennberg, P. O. and Zhou, X.:
863 Synthesis of the Southeast Atmosphere Studies: Investigating Fundamental Atmospheric
864 Chemistry Questions, *Bull. Am. Meteorol. Soc.*, 99(3), 547–567,
865 doi:10.1175/BAMS-D-16-0048.1, 2018.
- 866 Chen, Y., Xu, L., Humphry, T., Hettiyadura, A. P. S., Ovadnevaite, J., Huang, S., Poulain, L.,
867 Schroder, J. C., Campuzano-Jost, P., Jimenez, J. L., Herrmann, H., O’Dowd, C., Stone, E. A. and
868 Ng, N. L.: Response of the Aerodyne Aerosol Mass Spectrometer to Inorganic Sulfates and
869 Organosulfur Compounds: Applications in Field and Laboratory Measurements, *Environ. Sci.*
870 *Technol.*, 53(9), 5176–5186, doi:10.1021/acs.est.9b00884, 2019.
- 871 Clegg, S. L., Brimblecombe, P. and Wexler, A. S.: Thermodynamic Model of the System H +
872 -NH₄⁺ -SO₄²⁻ -NO₃⁻ -H₂O at Tropospheric Temperatures, , 5639(3), 2137–2154, 1998a.
- 873 Clegg, S. L., Brimblecombe, P. and Wexler, A. S.: Thermodynamic Model of the System H
874 -NH₄⁺ -SO₄²⁻ -NO₃⁻ -H₂O at Tropospheric Temperatures, *The Journal of Physical Chemistry*
875 *A*, 102(12), 2137–2154, doi:10.1021/jp973042r, 1998b.
- 876 Clegg, S. L., Seinfeld, J. H. and Edney, E. O.: Thermodynamic modelling of aqueous aerosols
877 containing electrolytes and dissolved organic compounds. II. An extended
878 Zdanovskii–Stokes–Robinson approach, *J. Aerosol Sci.*, 34(6), 667–690,
879 doi:10.1016/S0021-8502(03)00019-3, 2003.
- 880 Craig, R. L., Peterson, P. K., Nandy, L., Lei, Z., Hossain, M. A., Camarena, S., Dodson, R. A.,
881 Cook, R. D., Dutcher, C. S. and Ault, A. P.: Direct Determination of Aerosol pH: Size-Resolved
882 Measurements of Submicrometer and Supermicrometer Aqueous Particles, *Anal. Chem.*, 90(19),
883 11232–11239, doi:10.1021/acs.analchem.8b00586, 2018.
- 884 Crounse, J. D., McKinney, K. A., Kwan, A. J. and Wennberg, P. O.: Measurement of gas-phase
885 hydroperoxides by chemical ionization mass spectrometry, *Anal. Chem.*, 78(19), 6726–6732,
886 doi:10.1021/ac0604235, 2006.
- 887 Cubison, M. J., Ortega, A. M., Hayes, P. L., Farmer, D. K., Day, D., Lechner, M. J., Brune, W.
888 H., Apel, E., Diskin, G. S., Fisher, J. A. and Others: Effects of aging on organic aerosol from
889 open biomass burning smoke in aircraft and laboratory studies, *Atmos. Chem. Phys.*, 11(23),
890 12049–12064 [online] Available from:



- 891 <https://www.atmos-chem-phys.net/11/12049/2011/acp-11-12049-2011.pdf>, 2011.
- 892 DeCarlo, P. F., Kimmel, J. R., Trimborn, A., Northway, M. J., Jayne, J. T., Aiken, A. C., Gonin,
893 M., Fuhrer, K., Horvath, T., Docherty, K. S., Worsnop, D. R. and Jimenez, J. L.:
894 Field-deployable, high-resolution, time-of-flight aerosol mass spectrometer, *Anal. Chem.*,
895 78(24), 8281–8289, doi:10.1021/ac061249n, 2006.
- 896 DeCarlo, P. F., Dunlea, E. J., Kimmel, J. R., Aiken, A. C., Sueper, D., Crouse, J., Wennberg, P.
897 O., Emmons, L., Shinozuka, Y., Clarke, A. and Others: Fast airborne aerosol size and chemistry
898 measurements above Mexico City and Central Mexico during the MILAGRO campaign, 1foldr
899 Import 2019-10-08 Batch 1 [online] Available from:
900 <https://oaktrust.library.tamu.edu/bitstream/handle/1969.1/178622/document-2.pdf?sequence=2>,
901 2008.
- 902 Dentener, F. J. and Crutzen, P. J.: A three-dimensional model of the global ammonia cycle, *J.*
903 *Atmos. Chem.*, 19(4), 331–369, doi:10.1007/BF00694492, 1994.
- 904 Docherty, K. S., Lewandowski, M. and Jimenez, J. L.: Effect of Vaporizer Temperature on
905 Ambient Non-Refractory Submicron Aerosol Composition and Mass Spectra Measured by the
906 Aerosol Mass Spectrometer, *Aerosol Sci. Technol.*, 49(7), 485–494,
907 doi:10.1080/02786826.2015.1042100, 2015.
- 908 Dockery, D. W., Cunningham, J., Damokosh, A. I., Neas, L. M., Spengler, J. D., Koutrakis, P.,
909 Ware, J. H., Raizenne, M. and Speizer, F. E.: Health effects of acid aerosols on North American
910 children: respiratory symptoms, *Environ. Health Perspect.*, 104(5), 500–505,
911 doi:10.1289/ehp.96104500, 1996.
- 912 Dovrou, E., Lim, C. Y., Canagaratna, M. R., Kroll, J. H., Worsnop, D. R. and Keutsch, F. N.:
913 Measurement techniques for identifying and quantifying hydroxymethanesulfonate (HMS) in an
914 aqueous matrix and particulate matter using aerosol mass spectrometry and ion chromatography,
915 *Atmospheric Measurement Techniques*, 12(10), 5303–5315, doi:10.5194/amt-12-5303-2019,
916 2019.
- 917 Dunlea, E. J., DeCarlo, P. F., Aiken, A. C., Kimmel, J. R., Peltier, R. E., Weber, R. J., Tomlinson,
918 J., Collins, D. R., Shinozuka, Y., McNaughton, C. S. and Others: Evolution of Asian aerosols
919 during transpacific transport in INTEX-B, *Atmos. Chem. Phys.*, 9(19), 7257–7287 [online]
920 Available from: <https://www.atmos-chem-phys.net/9/7257/2009/acp-9-7257-2009.pdf>, 2009.
- 921 Facchini, M. C., Decesari, S., Rinaldi, M., Carbone, C., Finessi, E., Mircea, M., Fuzzi, S.,
922 Moretti, F., Tagliavini, E., Ceburnis, D. and O’Dowd, C. D.: Important source of marine
923 secondary organic aerosol from biogenic amines, *Environ. Sci. Technol.*, 42(24), 9116–9121,
924 doi:10.1021/es8018385, 2008.
- 925 Farmer, D. K., Matsunaga, A., Docherty, K. S., Surratt, J. D., Seinfeld, J. H., Ziemann, P. J. and
926 Jimenez, J. L.: Response of an aerosol mass spectrometer to organonitrates and organosulfates
927 and implications for atmospheric chemistry, *Proc. Natl. Acad. Sci. U. S. A.*, 107(15), 6670–6675,



- 928 doi:10.1073/pnas.0912340107, 2010.
- 929 Fountoukis, C. and Nenes, A.: ISORROPIA II: a computationally efficient thermodynamic
930 equilibrium model for $K^+Ca^{2+}Mg^{2+}NH_4^+Na^+SO_4^{2-}NO_3^-Cl^-H_2O$ aero, *Atmos. Chem.*
931 *Phys.*, 7(17), 4639–4659, doi:10.5194/acp-7-4639-2007, 2007.
- 932 Friese, E. and Ebel, A.: Temperature Dependent Thermodynamic Model of the System $H-NH_4$
933 $-Na-SO_4-NO_3-Cl-H_2O$, *The Journal of Physical Chemistry A*, 114(43), 11595–11631,
934 doi:10.1021/jp101041j, 2010.
- 935 Frossard, A. a., Russell, L. M., Burrows, S. M., Elliott, S. M., Bates, T. S. and Quinn, P. K.:
936 Sources and Composition of Submicron Organic Mass in Marine Aerosol Particles, *J. Geophys.*
937 *Res. D: Atmos.*, doi:10.1002/2014JD021913, 2014.
- 938 Froyd, K. D., Murphy, D. M., Sanford, T. J., Thomson, D. S., Wilson, J. C., Pfister, L. and Lait,
939 L.: Aerosol composition of the tropical upper troposphere, *Atmos. Chem. Phys.*, 9(13),
940 4363–4385, doi:10.5194/acp-9-4363-2009, 2009.
- 941 Froyd, K. D., Murphy, D. M., Brock, C. A., Campuzano-Jost, P., Dibb, J. E., Jimenez, J.-L.,
942 Kupc, A., Middlebrook, A. M., Schill, G. P., Thornhill, K. L., Williamson, C. J., Wilson, J. C.
943 and Ziemba, L. D.: A new method to quantify mineral dust and other aerosol species from
944 aircraft platforms using single-particle mass spectrometry, *Atmospheric Measurement*
945 *Techniques*, 12(11), 6209–6239, doi:10.5194/amt-12-6209-2019, 2019.
- 946 Fry, J. L., Draper, D. C., Zarzana, K. J., Campuzano-Jost, P., Day, D. A., Jimenez, J. L., Brown,
947 S. S., Cohen, R. C., Kaser, L., Hansel, A., Cappellin, L., Karl, T., Hodzic Roux, A., Turnipseed,
948 A., Cantrell, C., Lefer, B. L. and Grossberg, N.: Observations of gas- and aerosol-phase organic
949 nitrates at BEACHON-RoMBAS 2011, *Atmospheric Chemistry and Physics*, 13(17),
950 8585–8605, doi:10.5194/acp-13-8585-2013, 2013.
- 951 Gaston, C. J., Riedel, T. P., Zhang, Z., Gold, A., Surratt, J. D. and Thornton, J. A.: Reactive
952 Uptake of an Isoprene-Derived Epoxydiol to Submicron Aerosol Particles, ,
953 doi:10.1021/es5034266, 2014.
- 954 Gelaro, R., McCarty, W., Suárez, M. J., Todling, R., Molod, A., Takacs, L., Randles, C. A.,
955 Darmenov, A., Bosilovich, M. G., Reichle, R., Wargan, K., Coy, L., Cullather, R., Draper, C.,
956 Akella, S., Buchard, V., Conaty, A., da Silva, A. M., Gu, W., Kim, G.-K., Koster, R., Lucchesi,
957 R., Merkova, D., Nielsen, J. E., Partyka, G., Pawson, S., Putman, W., Rienecker, M., Schubert, S.
958 D., Sienkiewicz, M. and Zhao, B.: The Modern-Era Retrospective Analysis for Research and
959 Applications, Version 2 (MERRA-2), *J. Clim.*, 30(14), 5419–5454,
960 doi:10.1175/JCLI-D-16-0758.1, 2017.
- 961 Ge, X., Shaw, S. L. and Zhang, Q.: Toward Understanding Amines and Their Degradation
962 Products from Postcombustion CO₂ Capture Processes with Aerosol Mass Spectrometry,
963 *Environ. Sci. Technol.* [online] Available from: <http://pubs.acs.org/doi/abs/10.1021/es4056966>,
964 2014.



- 965 Gibb, S. W., Mantoura, R. F. C. and Liss, P. S.: Ocean-atmosphere exchange and atmospheric
966 speciation of ammonia and methylamines in the region of the NW Arabian Sea, *Global*
967 *Biogeochemical Cycles*, 13(1), 161–178, doi:10.1029/98gb00743, 1999.
- 968 Giglio, L., Randerson, J. T. and van der Werf, G. R.: Analysis of daily, monthly, and annual
969 burned area using the fourth-generation global fire emissions database (GFED4), *Journal of*
970 *Geophysical Research: Biogeosciences*, 118(1), 317–328 [online] Available from:
971 <https://agupubs.onlinelibrary.wiley.com/doi/abs/10.1002/jgrg.20042>, 2013.
- 972 Guo, H., Xu, L., Bougiatioti, A., Cerully, K. M., Capps, S. L., Hite, J. R., Jr, Carlton, A. G., Lee,
973 S.-H., Bergin, M. H., Ng, N. L. and Others: Fine-particle water and pH in the southeastern
974 United States, *Atmospheric Chemistry & Physics*, 15(9) [online] Available from:
975 [https://www.researchgate.net/profile/Kate_Cerully/publication/276206260_Fine-particle_water_](https://www.researchgate.net/profile/Kate_Cerully/publication/276206260_Fine-particle_water_and_pH_in_the_southeastern_United_States/links/55f6fc8508aeb1d9eee4213.pdf)
976 [and_pH_in_the_southeastern_United_States/links/55f6fc8508aeb1d9eee4213.pdf](https://www.researchgate.net/profile/Kate_Cerully/publication/276206260_Fine-particle_water_and_pH_in_the_southeastern_United_States/links/55f6fc8508aeb1d9eee4213.pdf), 2015.
- 977 Guo, H., Sullivan, A. P., Campuzano-Jost, P., Schroder, J. C., Lopez-Hilfiker, F. D., Dibb, J. E.,
978 Jimenez, J. L., Thornton, J. A., Brown, S. S., Nenes, A. and Others: Fine particle pH and the
979 partitioning of nitric acid during winter in the northeastern United States, *J. Geophys. Res. D:*
980 *Atmos.*, 121(17), 10–355 [online] Available from:
981 <https://onlinelibrary.wiley.com/doi/pdf/10.1002/2016JD025311>, 2016.
- 982 Guo, H., Liu, J., Froyd, K. D., Roberts, J. M., Veres, P. R., Hayes, P. L., Jimenez, J. L., Nenes, A.
983 and Weber, R. J.: Fine particle pH and gas–particle phase partitioning of inorganic species in
984 Pasadena, California, during the 2010 CalNex campaign, *Atmospheric Chemistry and Physics*,
985 17(9), 5703–5719, doi:10.5194/acp-17-5703-2017, 2017.
- 986 Guo, H., Campuzano-Jost, P., Nault, B. A., Day, D. A., Schroder, J. C., Dibb, J. E., Dollner, M.,
987 Weinzierl, B. and Jimenez, J. L.: The Importance of Size Ranges in Aerosol Instrument
988 Intercomparisons: A Case Study for the ATom Mission, , doi:10.5194/amt-2020-224, 2020.
- 989 Hennigan, C. J., Sullivan, A. P., Fountoukis, C. I., Nenes, A., Hecobian, A., Vargas, O., Hanks,
990 A. T. C., Huey, L. G., Lefer, B. L., Russell, A. G. and Others: On the volatility and production
991 mechanisms of newly formed nitrate and water soluble organic aerosol in Mexico City, [online]
992 Available from: <https://hal.archives-ouvertes.fr/hal-00304021/>, 2008.
- 993 Hennigan, C. J., Izumi, J., Sullivan, A. P., Weber, R. J. and Nenes, A.: A critical evaluation of
994 proxy methods used to estimate the acidity of atmospheric particles, *Atmos. Chem. Phys.*, 15(5),
995 2775 [online] Available from:
996 <https://pdfs.semanticscholar.org/18b0/f81231da34dbf1e29d753ae7c5e111cbd7fb.pdf>, 2015.
- 997 Hodshire, A. L., Campuzano-Jost, P., Kodros, J. K., Croft, B., Nault, B. A., Schroder, J. C.,
998 Jimenez, J. L. and Pierce, J. R.: The potential role of methanesulfonic acid (MSA) in aerosol
999 formation and growth and the associated radiative forcings, *Atmos. Chem. Phys.*, 19(5),
1000 3137–3160, doi:10.5194/acp-19-3137-2019, 2019.
- 1001 Hodzic, A., Campuzano-Jost, P., Bian, H., Chin, M., Colarco, P. R., Day, D. A., Froyd, K. D.,



- 1002 Heinold, B., Jo, D. S., Katich, J. M. and Others: Characterization of Organic Aerosol across the
1003 Global Remote Troposphere: A comparison of ATom measurements and global chemistry
1004 models, *Atmos. Chem. Phys.*, 2020.
- 1005 Hoesly, R. M., Smith, S. J., Feng, L., Klimont, Z., Janssens-Maenhout, G., Pitkanen, T., Seibert,
1006 J. J., Vu, L., Andres, R. J., Bolt, R. M. and Others: Historical (1750--2014) anthropogenic
1007 emissions of reactive gases and aerosols from the Community Emissions Data System (CEDS),
1008 *Geoscientific Model Development (Online)*, 11(PNNL-SA-123932) [online] Available from:
1009 <https://www.osti.gov/biblio/1421326>, 2018.
- 1010 Huang, S., Poulain, L., van Pinxteren, D., van Pinxteren, M., Wu, Z., Herrmann, H. and
1011 Wiedensohler, A.: Latitudinal and Seasonal Distribution of Particulate MSA over the Atlantic
1012 using a Validated Quantification Method with HR-ToF-AMS, *Environ. Sci. Technol.*, 51(1),
1013 418–426, doi:10.1021/acs.est.6b03186, 2017.
- 1014 Huffman, J. A., Jayne, J. T., Drewnick, F., Aiken, A. C., Onasch, T., Worsnop, D. R. and
1015 Jimenez, J. L.: Design, Modeling, Optimization, and Experimental Tests of a Particle Beam
1016 Width Probe for the Aerodyne Aerosol Mass Spectrometer, *Aerosol Sci. Technol.*, 39(12),
1017 1143–1163, doi:10.1080/02786820500423782, 2005.
- 1018 Hu, W., Campuzano-Jost, P., Day, D. A., Croteau, P., Canagaratna, M. R., Jayne, J. T., Worsnop,
1019 D. R. and Jimenez, J. L.: Evaluation of the new capture vaporizer for aerosol mass spectrometers
1020 (AMS) through field studies of inorganic species, *Aerosol Sci. Technol.*, 51(6), 735–754,
1021 doi:10.1080/02786826.2017.1296104, 2017a.
- 1022 Hu, W., Campuzano-Jost, P., Day, D. A., Croteau, P., Canagaratna, M. R., Jayne, J. T., Worsnop,
1023 D. R. and Jimenez, J. L.: Evaluation of the new capture vapourizer for aerosol mass
1024 spectrometers (AMS) through laboratory studies of inorganic species, *Atmospheric Measurement
1025 Techniques*, 10(8), doi:10.5194/amt-10-2897-2017, 2017b.
- 1026 Hu, W., Campuzano-Jost, P., Day, D. A., Nault, B., Park, T., Lee, T., Pajunoja, A., Virtanen, A.,
1027 Croteau, P. L., Canagaratna, M. R., Jayne, J. T., Worsnop, D. R. and Jimenez, J. L.: Ambient
1028 quantification and size distributions for organic aerosol (OA) in aerosol mass spectrometer
1029 (AMS) instruments with the new capture vaporizer (CV), *ACS Earth and Space Chemistry*,
1030 doi:10.1021/acsearthspacechem.9b00310, 2020.
- 1031 Hu, W. W., Campuzano-Jost, P., Palm, B. B., Day, D. A., Ortega, A. M., Hayes, P. L., Krechmer,
1032 J. E., Chen, Q., Kuwata, M., Liu, Y. J. and Others: Characterization of a real-time tracer for
1033 isoprene epoxydiols-derived secondary organic aerosol (IEPOX-SOA) from aerosol mass
1034 spectrometer measurements, *Atmos. Chem. Phys.*, 15(20), 11807–11833 [online] Available from:
1035 <https://www.atmos-chem-phys.net/15/11807/2015/acp-15-11807-2015.html>, 2015.
- 1036 IPCC: IPCC 2013: Climate Change 2013: The Physical Science Basis. Contribution of Working
1037 Group I to the Fifth Assessment Report of the Intergovernmental Panel on Climate Change,
1038 edited by T. F. Stocker, D. Qin, G. K. Plattner, M. Tignor, S. K. Allen, V. Bex, and P. M.
1039 Midgley, Cambridge University Press, Cambridge, United Kingdom and New York, NY, USA.,



1040 2013.

1041 Jang, M., Czoschke, N. M., Lee, S. and Kamens, R. M.: Heterogeneous atmospheric aerosol
1042 production by acid-catalyzed particle-phase reactions, *Science*, 298(5594), 814–817,
1043 doi:10.1126/science.1075798, 2002.

1044 Jayne, J. T., Leard, D. C., Zhang, X., Davidovits, P., Smith, K. A., Kolb, C. E. and Worsnop, D.
1045 R.: Development of an Aerosol Mass Spectrometer for Size and Composition Analysis of
1046 Submicron Particles, *Aerosol Sci. Technol.*, 33(1-2), 49–70, doi:10.1080/027868200410840,
1047 2000.

1048 Jimenez, J. L., Canagaratna, M. R., Donahue, N. M., Prevot, A. S. H., Zhang, Q., Kroll, J. H.,
1049 DeCarlo, P. F., Allan, J. D., Coe, H., Ng, N. L., Aiken, A. C., Docherty, K. S., Ulbrich, I. M.,
1050 Grieshop, A. P., Robinson, A. L., Duplissy, J., Smith, J. D., Wilson, K. R., Lanz, V. A., Hueglin,
1051 C., Sun, Y. L., Tian, J., Laaksonen, A., Raatikainen, T., Rautiainen, J., Vaattovaara, P., Ehn, M.,
1052 Kulmala, M., Tomlinson, J. M., Collins, D. R., Cubison, M. J., Dunlea, E. J., Huffman, J. A.,
1053 Onasch, T. B., Alfarra, M. R., Williams, P. I., Bower, K., Kondo, Y., Schneider, J., Drewnick, F.,
1054 Borrmann, S., Weimer, S., Demerjian, K., Salcedo, D., Cottrell, L., Griffin, R., Takami, A.,
1055 Miyoshi, T., Hatakeyama, S., Shimono, A., Sun, J. Y., Zhang, Y. M., Dzepina, K., Kimmel, J. R.,
1056 Sueper, D., Jayne, J. T., Herndon, S. C., Trimborn, A. M., Williams, L. R., Wood, E. C.,
1057 Middlebrook, A. M., Kolb, C. E., Baltensperger, U. and Worsnop, D. R.: Evolution of organic
1058 aerosols in the atmosphere, *Science*, 326(5959), 1525–1529, doi:10.1126/science.1180353, 2009.

1059 Jo, D. S., Hodzic, A., Emmons, L. K., Marais, E. A., Peng, Z., Nault, B. A., Hu, W.,
1060 Campuzano-Jost, P. and Jimenez, J. L.: A simplified parameterization of
1061 isoprene-epoxydiol-derived secondary organic aerosol (IEPOX-SOA) for global chemistry and
1062 climate models: a case study with GEOS-Chem v11-02-rc, *Geoscientific Model Development*,
1063 12(7), 2983–3000, doi:10.5194/gmd-12-2983-2019, 2019.

1064 Johnson, K. S., Laskin, A., Jimenez, J. L., Shutthanandan, V., Molina, L. T., Salcedo, D.,
1065 Dzepina, K. and Molina, M. J.: Comparative analysis of urban atmospheric aerosol by
1066 particle-induced X-ray emission (PIXE), proton elastic scattering analysis (PESA), and aerosol
1067 mass spectrometry (AMS), *Environ. Sci. Technol.*, 42(17), 6619–6624, doi:10.1021/es800393e,
1068 2008.

1069 Kang et al.: Secondary organic aerosol mass yields from the dark NO₃ oxidation of α -pinene and
1070 Δ -carene: effect of RO₂ radical fate, 2016.

1071 Keene, W. C.: Variation of marine aerosol acidity with particle size, *Geophys. Res. Lett.*, 29(7),
1072 20,565, doi:10.1029/2001GL013881, 2002.

1073 Lambert, J. B.: *Organic structural spectroscopy*, Pearson College Division., 1998.

1074 Lee, B. H., Lopez-Hilfiker, F. D., Mohr, C., Kurtén, T., Worsnop, D. R. and Thornton, J. a.: An
1075 iodide-adduct high-resolution time-of-flight chemical-ionization mass spectrometer: application
1076 to atmospheric inorganic and organic compounds, *Environ. Sci. Technol.*, 48(11), 6309–6317,



1077 doi:10.1021/es500362a, 2014.

1078 Lee, B. H., Lopez-Hilfiker, F. D., Veres, P. R., McDuffie, E. E., Fibiger, D. L., Sparks, T. L.,
1079 Ebben, C. J., Green, J. R., Schroder, J. C., Campuzano-Jost, P. and Others: Flight deployment of
1080 a high-resolution time-of-flight chemical ionization mass spectrometer: Observations of reactive
1081 halogen and nitrogen oxide species, *J. Geophys. Res. D: Atmos.*, 123(14), 7670–7686 [online]
1082 Available from:
1083 [https://agupubs.onlinelibrary.wiley.com/doi/abs/10.1029/2017JD028082@10.1002/\(ISSN\)2169-](https://agupubs.onlinelibrary.wiley.com/doi/abs/10.1029/2017JD028082@10.1002/(ISSN)2169-)
1084 8996.WINTER1, 2018.

1085 Lee, T., Sullivan, A. P., Mack, L., Jimenez, J. L., Kreidenweis, S. M., Onasch, T. B., Worsnop, D.
1086 R., Malm, W., Wold, C. E., Hao, W. M. and Collett, J. L.: Chemical Smoke Marker Emissions
1087 During Flaming and Smoldering Phases of Laboratory Open Burning of Wildland Fuels, *Aerosol*
1088 *Sci. Technol.*, 44(9), i–v, doi:10.1080/02786826.2010.499884, 2010.

1089 Liao, J., Froyd, K. D., Murphy, D. M., Keutsch, F. N., Yu, G., Wennberg, P. O., Clair, J. M. S.,
1090 Crouse, J. D., Wisthaler, A., Mikoviny, T. and Others: Airborne measurements of
1091 organosulfates over the continental US, *J. Geophys. Res. D: Atmos.*, 120(7), 2990–3005 [online]
1092 Available from:
1093 <https://agupubs.onlinelibrary.wiley.com/doi/abs/10.1002/2014JD022378%4010.1002/%28ISSN>
1094 [%292169-8996.SEAFOURC1](https://agupubs.onlinelibrary.wiley.com/doi/abs/10.1002/2014JD022378%4010.1002/%28ISSN), 2015.

1095 Li, G., Bei, N., Cao, J., Huang, R., Wu, J., Feng, T., Wang, Y., Liu, S., Zhang, Q., Tie, X. and
1096 Molina, L. T.: A possible pathway for rapid growth of sulfate during haze days in China, ,
1097 3301–3316 [online] Available from: <https://dspace.mit.edu/handle/1721.1/109728?show=full>
1098 (Accessed 2 August 2019), 2017.

1099 Lighty, J. S., Veranth, J. M. and Sarofim, A. F.: Combustion aerosols: factors governing their size
1100 and composition and implications to human health, *J. Air Waste Manag. Assoc.*, 50(9),
1101 1565–618; discussion 1619–22 [online] Available from:
1102 <https://www.ncbi.nlm.nih.gov/pubmed/11055157>, 2000.

1103 Liu, P., Ziemann, P. J., Kittelson, D. B. and McMurry, P. H.: Generating Particle Beams of
1104 Controlled Dimensions and Divergence: II. Experimental Evaluation of Particle Motion in
1105 Aerodynamic Lenses and Nozzle Expansions, *Aerosol Sci. Technol.*, 22(3), 314–324,
1106 doi:10.1080/02786829408959749, 1995.

1107 Liu, X., Day, D. A., Krechmer, J. E., Brown, W., Peng, Z., Ziemann, P. J. and Jimenez, J. L.:
1108 Direct measurements of semi-volatile organic compound dynamics show near-unity mass
1109 accommodation coefficients for diverse aerosols, *Communications Chemistry*, 2(1), 1–9,
1110 doi:10.1038/s42004-019-0200-x, 2019.

1111 Lohmann, U., Broekhuizen, K., Leaitch, R., Shantz, N. and Abbatt, J.: How efficient is cloud
1112 droplet formation of organic aerosols?, *Geophys. Res. Lett.*, 31(5), 2004.

1113 Losey, D. J., Ott, E.-J. E. and Freedman, M. A.: Effects of High Acidity on Phase Transitions of



- 1114 an Organic Aerosol, *J. Phys. Chem. A*, 122(15), 3819–3828, doi:10.1021/acs.jpca.8b00399,
1115 2018.
- 1116 Massucci, M., Clegg, S. L. and Brimblecombe, P.: Equilibrium Partial Pressures,
1117 Thermodynamic Properties of Aqueous and Solid Phases, and Cl₂ Production from Aqueous
1118 HCl and HNO₃ and Their Mixtures, *J. Phys. Chem. A*, 103(21), 4209–4226,
1119 doi:10.1021/jp9847179, 1999.
- 1120 Matthew, B. M., Middlebrook, A. M. and Onasch, T. B.: Collection Efficiencies in an Aerodyne
1121 Aerosol Mass Spectrometer as a Function of Particle Phase for Laboratory Generated Aerosols,
1122 *Aerosol Sci. Technol.*, 42(11), 884–898, doi:10.1080/02786820802356797, 2008.
- 1123 Meskhidze, N., Chameides, W. L., Nenes, A. and Chen, G.: Iron mobilization in mineral dust:
1124 Can anthropogenic SO₂ emissions affect ocean productivity?, *Geophys. Res. Lett.*, 30(21)
1125 [online] Available from:
1126 <https://agupubs.onlinelibrary.wiley.com/doi/abs/10.1029/2003GL018035>, 2003.
- 1127 Middlebrook, A. M., Bahreini, R., Jimenez, J. L. and Canagaratna, M. R.: Evaluation of
1128 Composition-Dependent Collection Efficiencies for the Aerodyne Aerosol Mass Spectrometer
1129 using Field Data, *Aerosol Sci. Technol.*, 46(3), 258–271, doi:10.1080/02786826.2011.620041,
1130 2012.
- 1131 Müller, C., Iinuma, Y., Karstensen, J., Van Pinxteren, D., Lehmann, S., Gnauk, T. and Herrmann,
1132 H.: Seasonal variation of aliphatic amines in marine sub-micrometer particles at the Cape Verde
1133 islands, [online] Available from: <https://oar.tib.eu/jspui/handle/123456789/261>, 2009.
- 1134 Murphy, S. M., Sorooshian, A., Kroll, J. H., Ng, N. L., Chhabra, P., Tong, C., Surratt, J. D.,
1135 Knipping, E., Flagan, R. C. and Seinfeld, J. H.: Secondary aerosol formation from atmospheric
1136 reactions of aliphatic amines, *Atmospheric Chemistry and Physics Discussions*, 7(1), 289–349,
1137 doi:10.5194/acpd-7-289-2007, 2007.
- 1138 Nault, B. A., Campuzano-Jost, P., Day, D. A., Schroder, J. C., Anderson, B., Beyersdorf, A. J.,
1139 Blake, D. R., Brune, W. H., Choi, Y., Corr, C. A., Gouw, J. A. de, Dibb, J., DiGangi, J. P., Diskin,
1140 G. S., Fried, A., Huey, L. G., Kim, M. J., Knute, C. J., Lamb, K. D., Lee, T., Park, T., Pusede, S.
1141 E., Scheuer, E., Thornhill, K. L., Woo, J.-H. and Jimenez, J. L.: Secondary organic aerosol
1142 production from local emissions dominates the organic aerosol budget over Seoul, South Korea,
1143 during KORUS-AQ, *Atmos. Chem. Phys.*, 18(24), 17769–17800,
1144 doi:10.5194/acp-18-17769-2018, 2018.
- 1145 Nault, B. A., Campuzano-Jost, P., Jo, D., Day, D., Bahreini, R., Bian, H., Chin, M., Clegg, S.,
1146 Colarco, P., Kodros, J., Lopez-Hilfiker, F., Marais, E., Middlebrook, A., Neuman, A., Nowak, J.,
1147 Pierce, J., Thornton, J., Tsigaridis, K., Jimenez, J. and ATom Science Team: Global Survey of
1148 Aerosol Acidity from Polluted to Remote Locations: Measurements and Comparisons with
1149 Global Models, display, doi:10.5194/egusphere-egu2020-11366, 2020.
- 1150 Nenes, A., Pandis, S. N. and Pilinis, C.: Continued development and testing of a new



- 1151 thermodynamic aerosol module for urban and regional air quality models, *Atmos. Environ.*,
1152 33(10), 1553–1560, doi:10.1016/S1352-2310(98)00352-5, 1999.
- 1153 Ng, N. L., Herndon, S. C., Trimborn, A., Canagaratna, M. R., Croteau, P. L., Onasch, T. B.,
1154 Sueper, D., Worsnop, D. R., Zhang, Q., Sun, Y. L. and Jayne, J. T.: An Aerosol Chemical
1155 Speciation Monitor (ACSM) for Routine Monitoring of the Composition and Mass
1156 Concentrations of Ambient Aerosol, *Aerosol Sci. Technol.*, 45(7), 780–794,
1157 doi:10.1080/02786826.2011.560211, 2011a.
- 1158 Ng, N. L., Canagaratna, M. R., Jimenez, J. L., Chhabra, P. S., Seinfeld, J. H. and Worsnop, D. R.:
1159 Changes in organic aerosol composition with aging inferred from aerosol mass spectra, *Atmos.*
1160 *Chem. Phys.*, 11(13), 6465 [online] Available from:
1161 <http://citeseerx.ist.psu.edu/viewdoc/download?doi=10.1.1.388.4858&rep=rep1&type=pdf>,
1162 2011b.
- 1163 Ovadnevaite, J., Ceburnis, D., Canagaratna, M., Berresheim, H., Bialek, J., Martucci, G.,
1164 Worsnop, D. R. and O'Dowd, C.: On the effect of wind speed on submicron sea salt mass
1165 concentrations and source fluxes, *J. Geophys. Res. D: Atmos.*, 117(D16) [online] Available
1166 from: <https://agupubs.onlinelibrary.wiley.com/doi/abs/10.1029/2011JD017379>, 2012.
- 1167 Paulot, F., Jacob, D. J., Johnson, M. T., Bell, T. G., Baker, A. R., Keene, W. C., Lima, I. D.,
1168 Doney, S. C. and Stock, C. A.: Global oceanic emission of ammonia: Constraints from seawater
1169 and atmospheric observations, *Global Biogeochem. Cycles*, 29(8), 1165–1178,
1170 doi:10.1002/2015GB005106, 2015.
- 1171 Phinney, L., Richard Leitch, W., Lohmann, U., Boudries, H., Worsnop, D. R., Jayne, J. T.,
1172 Toom-Saunty, D., Wadleigh, M., Sharma, S. and Shantz, N.: Characterization of the aerosol over
1173 the sub-arctic north east Pacific Ocean, *Deep Sea Res. Part 2 Top. Stud. Oceanogr.*, 53(20),
1174 2410–2433, doi:10.1016/j.dsr2.2006.05.044, 2006.
- 1175 van Pinxteren, M., Fiedler, B., van Pinxteren, D., Iinuma, Y., Körtzinger, A. and Herrmann, H.:
1176 Chemical characterization of sub-micrometer aerosol particles in the tropical Atlantic Ocean:
1177 marine and biomass burning influences, *J. Atmos. Chem.*, 72(2), 105–125,
1178 doi:10.1007/s10874-015-9307-3, 2015.
- 1179 Pye, H. O. T., Liao, H., Wu, S., Mickley, L. J., Jacob, D. J., Henze, D. K. and Seinfeld, J. H.:
1180 Effect of changes in climate and emissions on future sulfate-nitrate-ammonium aerosol levels in
1181 the United States, *J. Geophys. Res. D: Atmos.*, 114(D1) [online] Available from:
1182 <https://agupubs.onlinelibrary.wiley.com/doi/abs/10.1029/2008JD010701>, 2009.
- 1183 Pye, H. O. T., Nenes, A., Alexander, B., Ault, A. P., Barth, M. C., Clegg, S. L., Collett, J. L., Jr,
1184 Fahey, K. M., Hennigan, C. J., Herrmann, H. and Others: The Acidity of Atmospheric Particles
1185 and Clouds, UMBC Faculty Collection [online] Available from:
1186 <https://www.atmos-chem-phys-discuss.net/acp-2019-889/acp-2019-889.pdf>, 2019.
- 1187 Quinn, P. K., Charlson, R. J. and Bates, T. S.: Simultaneous observations of ammonia in the



- 1188 atmosphere and ocean, *Nature*, 335(6188), 336–338, doi:10.1038/335336a0, 1988.
- 1189 Quinn, P. K., Bates, T. S., Coffman, D., Onasch, T. B., Worsnop, D., Baynard, T., De Gouw, J.
1190 A., Goldan, P. D., Kuster, W. C., Williams, E. and Others: Impacts of sources and aging on
1191 submicrometer aerosol properties in the marine boundary layer across the Gulf of Maine, J.
1192 *Geophys. Res. D: Atmos.*, 111(D23) [online] Available from:
1193 <https://agupubs.onlinelibrary.wiley.com/doi/abs/10.1029/2006JD007582>, 2006.
- 1194 Raizenne, M., Neas, L. M., Damokosh, A. I., Dockery, D. W., Spengler, J. D., Koutrakis, P.,
1195 Ware, J. H. and Speizer, F. E.: Health effects of acid aerosols on North American children:
1196 pulmonary function, *Environ. Health Perspect.*, 104(5), 506–514, doi:10.1289/ehp.96104506,
1197 1996.
- 1198 Rindelaub, J. D., Craig, R. L., Nandy, L., Bondy, A. L., Dutcher, C. S., Shepson, P. B. and Ault,
1199 A. P.: Direct Measurement of pH in Individual Particles via Raman Microspectroscopy and
1200 Variation in Acidity with Relative Humidity, *J. Phys. Chem. A*, 120(6), 911–917,
1201 doi:10.1021/acs.jpca.5b12699, 2016.
- 1202 Riva, M., Budisulistiorini, S. H., Chen, Y., Zhang, Z., D’Ambro, E. L., Zhang, X., Gold, A.,
1203 Turpin, B. J., Thornton, J. A., Canagaratna, M. R. and Surratt, J. D.: Chemical Characterization
1204 of Secondary Organic Aerosol from Oxidation of Isoprene Hydroxyhydroperoxides, *Environ.*
1205 *Sci. Technol.*, *acs.est.6b02511–acs.est.6b02511*, doi:10.1021/acs.est.6b02511, 2016.
- 1206 Riva, M., Rantala, P., Krechmer, J. E., Peräkylä, O., Zhang, Y., Heikkinen, L., Garmash, O., Yan,
1207 C., Kulmala, M., Worsnop, D. and Ehn, M.: Evaluating the performance of five different
1208 chemical ionization techniques for detecting gaseous oxygenated organic species, *Atmospheric*
1209 *Measurement Techniques Discussions*, 12(4), 2403–2421, doi:10.5194/amt-12-2403-2019,
1210 2019a.
- 1211 Riva, M., Chen, Y., Zhang, Y., Lei, Z., Olson, N. E., Boyer, H. C., Narayan, S., Yee, L. D.,
1212 Green, H. S., Cui, T., Zhang, Z., Baumann, K., Fort, M., Edgerton, E., Budisulistiorini, S. H.,
1213 Rose, C. A., Ribeiro, I. O., E Oliveira, R. L., Dos Santos, E. O., Machado, C. M. D., Szopa, S.,
1214 Zhao, Y., Alves, E. G., de Sá, S. S., Hu, W., Knipping, E. M., Shaw, S. L., Duvoisin Junior, S.,
1215 Souza, R. A. F., Palm, B. B., Jimenez, J.-L., Glasius, M., Goldstein, A. H., Pye, H. O. T., Gold,
1216 A., Turpin, B. J., Vizuete, W., Martin, S. T., Thornton, J. A., Dutcher, C. S., Ault, A. P. and
1217 Surratt, J. D.: Increasing Isoprene Epoxydiol-to-Inorganic Sulfate Aerosol Ratio Results in
1218 Extensive Conversion of Inorganic Sulfate to Organosulfur Forms: Implications for Aerosol
1219 Physicochemical Properties, *Environ. Sci. Technol.*, 53(15), 8682–8694,
1220 doi:10.1021/acs.est.9b01019, 2019b.
- 1221 Salcedo, D., Onasch, T. B., Aiken, a. C., Williams, L. R., de Foy, B., Cubison, M. J., Worsnop,
1222 D. R., Molina, L. T. and Jimenez, J. L.: Determination of particulate lead using aerosol mass
1223 spectrometry: MILAGRO/MCMA-2006 observations, *Atmos. Chem. Phys.*, 10(12), 5371–5389,
1224 doi:10.5194/acp-10-5371-2010, 2010.
- 1225 Schindler, D. W.: Effects of Acid rain on freshwater ecosystems, *Science*, 239(4836), 149–157,



- 1226 doi:10.1126/science.239.4836.149, 1988.
- 1227 Schroder, J. C., Campuzano-Jost, P., Day, D. A., Shah, V., Larson, K., Sommers, J. M., Sullivan,
1228 A. P., Campos, T., Reeves, J. M., Hills, A., Hornbrook, R. S., Blake, N. J., Scheuer, E., Guo, H.,
1229 Fibiger, D. L., McDuffie, E. E., Hayes, P. L., Weber, R. J., Dibb, J. E., Apel, E. C., Jaeglé, L.,
1230 Brown, S. S., Thornton, J. A. and Jimenez, J. L.: Sources and Secondary Production of Organic
1231 Aerosols in the Northeastern United States during WINTER, *J. Geophys. Res. D: Atmos.*, 42,
1232 4478, doi:10.1029/2018JD028475, 2018.
- 1233 Seinfeld, J. H. and Pandis, S. N.: *Atmospheric Chemistry and Physics*, 2nd ed., John Wiley &
1234 Sons, Inc., New York., 2006.
- 1235 Song, S., Gao, M., Xu, W., Shao, J., Shi, G., Wang, S., Wang, Y., Sun, Y. and McElroy, M. B.:
1236 Fine-particle pH for Beijing winter haze as inferred from different thermodynamic equilibrium
1237 models, *Atmos. Chem. Phys.*, 18(10), 7423–7438, doi:10.5194/acp-18-7423-2018, 2018.
- 1238 Song, S., Gao, M., Xu, W., Sun, Y., Worsnop, D. R., Jayne, J. T., Zhang, Y., Zhu, L., Li, M.,
1239 Zhou, Z. and Others: Possible heterogeneous chemistry of hydroxymethanesulfonate (HMS) in
1240 northern China winter haze, *Atmos. Chem. Phys.*, 19(2), 1357–1371 [online] Available from:
1241 <https://www.atmos-chem-phys.net/19/1357/2019/acp-19-1357-2019.pdf>, 2019.
- 1242 Sorooshian, A., Padró, L. T., Nenes, A., Feingold, G., McComiskey, A., Hersey, S. P., Gates, H.,
1243 Jonsson, H. H., Miller, S. D., Stephens, G. L. and Others: On the link between ocean biota
1244 emissions, aerosol, and maritime clouds: Airborne, ground, and satellite measurements off the
1245 coast of California, *Global Biogeochem. Cycles*, 23(4) [online] Available from:
1246 <https://agupubs.onlinelibrary.wiley.com/doi/abs/10.1029/2009GB003464>, 2009.
- 1247 Sorooshian, A., Crosbie, E., Maudlin, L. C., Youn, J.-S., Wang, Z., Shingler, T., Ortega, A. M.,
1248 Hersey, S. and Woods, R. K.: Surface and airborne measurements of organosulfur and
1249 methanesulfonate over the western United States and coastal areas, *J. Geophys. Res. D: Atmos.*,
1250 120(16), 8535–8548, doi:10.1002/2015JD023822, 2015.
- 1251 Stith, J. L., Ramanathan, V., Cooper, W. A., Roberts, G. C., DeMott, P. J., Carmichael, G., Hatch,
1252 C. D., Adhikary, B., Twohy, C. H., Rogers, D. C., Baumgardner, D., Prenni, A. J., Campos, T.,
1253 Gao, R., Anderson, J. and Feng, Y.: An overview of aircraft observations from the Pacific Dust
1254 Experiment campaign, *J. Geophys. Res.*, 114(D5), 833, doi:10.1029/2008JD010924, 2009.
- 1255 Sueper, D.: ToF-AMS Data Analysis Software Webpage, [online] Available from:
1256 http://cires1.colorado.edu/jimenez-group/wiki/index.php/ToF-AMS_Analysis_Software
1257 (Accessed 4 January 2017), 2018.
- 1258 Surratt, J. D., Kroll, J. H., Kleindienst, T. E., Edney, E. O., Claeys, M., Sorooshian, A., Ng, N.
1259 L., Offenberg, J. H., Lewandowski, M., Jaoui, M., Flagan, R. C. and Seinfeld, J. H.: Evidence for
1260 organosulfates in secondary organic aerosol, *Environ. Sci. Technol.*, 41(2), 517–527,
1261 doi:10.1021/es062081q, 2007.
- 1262 Surratt, J. D., Gómez-González, Y., Chan, A. W. H., Vermeylen, R., Shahgholi, M., Kleindienst,



- 1263 T. E., Edney, E. O., Offenberg, J. H., Lewandowski, M., Jaoui, M., Maenhaut, W., Claeys, M.,
1264 Flagan, R. C. and Seinfeld, J. H.: Organosulfate formation in biogenic secondary organic aerosol,
1265 *J. Phys. Chem. A*, 112(36), 8345–8378, doi:10.1021/jp802310p, 2008.
- 1266 Thornton, J. A., Jaeglé, L. and McNeill, V. F.: Assessing known pathways for HO₂ loss in
1267 aqueous atmospheric aerosols: Regional and global impacts on tropospheric oxidants, *J.*
1268 *Geophys. Res. D: Atmos.*, 113(D5) [online] Available from:
1269 <https://agupubs.onlinelibrary.wiley.com/doi/abs/10.1029/2007JD009236>, 2008.
- 1270 Tolocka, M. P. and Turpin, B.: Contribution of organosulfur compounds to organic aerosol mass,
1271 *Environ. Sci. Technol.*, 46(15), 7978–7983, doi:10.1021/es300651v, 2012.
- 1272 Toon, O. B., Maring, H., Dibb, J., Ferrare, R., Jacob, D. J., Jensen, E. J., Luo, Z. J., Mace, G. G.,
1273 Pan, L. L., Pfister, L. and Others: Planning, implementation, and scientific goals of the Studies of
1274 Emissions and Atmospheric Composition, Clouds and Climate Coupling by Regional Surveys
1275 (SEAC4RS) field mission, *J. Geophys. Res. D: Atmos.*, 121(9), 4967–5009 [online] Available
1276 from:
1277 <https://agupubs.onlinelibrary.wiley.com/doi/abs/10.1002/2015JD024297%4010.1002/%28ISSN>
1278 <https://agupubs.onlinelibrary.wiley.com/doi/abs/10.1002/2015JD024297%4010.1002/%28ISSN>
1279 %292169-8996.SEAFOURC1, 2016.
- 1279 Wang, Y., Zhang, Q., Jiang, J., Zhou, W., Wang, B., He, K., Duan, F., Zhang, Q., Philip, S. and
1280 Xie, Y.: Enhanced sulfate formation during China's severe winter haze episode in January 2013
1281 missing from current models, *J. Geophys. Res. D: Atmos.*, 119(17), 10–425 [online] Available
1282 from: <https://agupubs.onlinelibrary.wiley.com/doi/abs/10.1002/2013JD021426>, 2014.
- 1283 Weber, R. J., Guo, H., Russell, A. G. and Nenes, A.: High aerosol acidity despite declining
1284 atmospheric sulfate concentrations over the past 15 years, *Nat. Geosci.*, 9, 282,
1285 doi:10.1038/ngeo2665, 2016.
- 1286 Wexler, A. S. and Clegg, S. L.: Atmospheric aerosol models for systems including the ions H⁺,
1287 NH₄⁺, Na⁺, SO₄²⁻, NO₃⁻, Cl⁻, Br⁻, and H₂O, *J. Geophys. Res. D: Atmos.*, 107(D14), ACH-14
1288 [online] Available from:
1289 <https://agupubs.onlinelibrary.wiley.com/doi/abs/10.1029/2001JD000451>, 2002.
- 1290 Youn, J.-S., Crosbie, E., Maudlin, L. C., Wang, Z. and Sorooshian, A.: Dimethylamine as a major
1291 alkyl amine species in particles and cloud water: Observations in semi-arid and coastal regions,
1292 *Atmos. Environ.*, 122, 250–258, doi:10.1016/j.atmosenv.2015.09.061, 2015.
- 1293 Zhang, Q., Stanier, C. O., Canagaratna, M. R., Jayne, J. T., Worsnop, D. R., Pandis, S. N. and
1294 Jimenez, J. L.: Insights into the chemistry of new particle formation and growth events in
1295 Pittsburgh based on aerosol mass spectrometry, *Environ. Sci. Technol.*, 38(18), 4797–4809,
1296 doi:10.1021/es035417u, 2004a.
- 1297 Zhang, Q., Jimenez, J. L., Worsnop, D. R. and Canagaratna, M.: A case study of urban particle
1298 acidity and its influence on secondary organic aerosol, *Environ. Sci. Technol.*, 41(9), 3213–3219,
1299 doi:10.1021/Es061812j, 2007a.



- 1300 Zhang, Q., Jimenez, J. L., Canagaratna, M. R., Allan, J. D., Coe, H., Ulbrich, I., Alfarra, M. R.,
1301 Takami, A., Middlebrook, A. M., Sun, Y. L. and Others: Ubiquity and dominance of oxygenated
1302 species in organic aerosols in anthropogenically-influenced Northern Hemisphere midlatitudes,
1303 *Geophys. Res. Lett.*, 34(13) [online] Available from:
1304 <https://agupubs.onlinelibrary.wiley.com/doi/abs/10.1029/2007GL029979>
1305 [%28ISSN%291944-8007.GRL40, 2007b](https://doi.org/10.1002/%28ISSN%291944-8007.GRL40,2007b).
- 1306 Zhang, X., Smith, K. A., Worsnop, D. R., Jimenez, J. L., Jayne, J. T., Kolb, C. E., Morris, J. and
1307 Davidovits, P.: Numerical Characterization of Particle Beam Collimation: Part II Integrated
1308 Aerodynamic-Lens-Nozzle System, *Aerosol Sci. Technol.*, 38(6), 619–638,
1309 doi:10.1080/02786820490479833, 2004b.
- 1310 Zheng, B., Zhang, Q., Zhang, Y., He, K. B., Wang, K., Zheng, G. J., Duan, F. K., Ma, Y. L. and
1311 Kimoto, T.: Heterogeneous chemistry: a mechanism missing in current models to explain
1312 secondary inorganic aerosol formation during the January 2013 haze episode in North China,
1313 *Atmospheric Chemistry and Physics Discussions*, 14(11), 16731–16776,
1314 doi:10.5194/acpd-14-16731-2014, 2014.
- 1315 Zheng, Y., Cheng, X., Liao, K., Li, Y., Li, Y., Huang, R.-J., Hu, W., Liu, Y., Zhu, T., Chen, S. and
1316 Others: Characterization of Anthropogenic Organic Aerosols by TOF-ACSM with the New
1317 Capture Vaporizer, *Atmospheric Measurement Techniques* [online] Available from:
1318 <https://www.atmos-meas-tech-discuss.net/amt-2019-449/amt-2019-449.pdf>, 2020.
- 1319 Zorn, S. R., Drewnick, F., Schott, M., Hoffmann, T. and Borrmann, S.: Characterization of the
1320 South Atlantic marine boundary layer aerosol using an aerodyne aerosol mass spectrometer,
1321 [online] Available from: <https://hal.archives-ouvertes.fr/hal-00304023/>, 2008.
- 1322